Master's Thesis

Master in Telecommunication Engineering

Design of a Ku Band filter using the extracted pole method

Ivan Baró Gutiérrez

Supervisor: Jordi Verdú Tirado

Department of Telecommunications and Systems engineering

Escola d'Enginyeria (EE)

Universitat Autònoma de Barcelona (UAB)

July 2019

El sotasignant, *Jordi Verdu Tirado*, Professor de l'Escola d'Enginyeria de la Universitat Autònoma de Barcelona (UAB),

CERTIFICA:

Que el projecte presentat en aquesta memòria de Treball Final de Master ha estat realitzat sota la seva direcció per l'alumne Iván Baró Gutiérrez.

I, perquè consti a tots els efectes, signa el present certificat.

Bellaterra, 03 del Juliol de 2019

Signatura: *Jordi Verdu Tirado*

Resum:

En aquest projecte es presenta l'estudi d'un filtre de transmissió compacte en banda Ku (12.7GHz a 14.7GHz) en tecnologia planar, utilitzant una topologia parell node ressonant, node no ressonant, basada en el mètode de pol extret, la qual ens permet generar zeros de transmissió independents de la resta de ressonadors.

En el document, es descriu la teoria utilitzada, el disseny, anàlisi, mesura i resultats de les diferents versions del filtre. Es realitzaran diferents anàlisis de tolerància per comprovar la sensibilitat del filtre i comparar-lo amb altres topologies que utilitzin via-holes.

Finalment la mesura del prototip fabricat i els resultats obtinguts mitjançant simulació seran correlats per validar el correcte funcionament de l'estructura.

Resumen:

En este proyecto se presenta el estudio de un filtro de transmisión compacto en banda Ku (12.7GHz a 14.7GHz) en tecnología planar, utilizando una topología par nodo resonante, nodo no resonante, basada en el método de polo extraído, la cual nos permite generar ceros de transmisión independientes del resto de resonadores.

En el documento, se describe la teoría utilizada, el diseño, análisis, medida y resultados de las diferentes versiones del filtro. Se realizarán diferentes análisis de tolerancia para comprobar la sensibilidad del filtro y compararlo con otras topologías que utilicen via-holes.

Finalmente la medida del prototipo fabricado y los resultados obtenidos mediante simulación serán correlados para validar el correcto funcionamiento de la estructura.

Summary:

This project presents the study of a compact transmission filter in Ku band (12.7GHz to 14.7GHz) in planar technology, using a non-resonator node topology with dangling resonator based on the extracted pole method, which allows us to generate transmission zeros independent of the rest of the resonators.

In the document, the used theory, the design, analysis, measurement and results of the different versions of the filter are described. Different tolerance analysis will be carried out to check the sensitivity of the filter and compare it with other topologies that use via-holes.

Finally the measurement of the manufactured prototype and the results obtained by simulation will be correlated to validate the correct performance of the structure.

Index

List of Figures **9**

List of Tables **12**

1. Introduction **13**

2. Filter Theory **15**

2.1 Characterization of Lossless Low pass prototype Filter Functions 15

2.2 Synthesis of a Generalized Chebyshev Filtering Function 18

2.3 General extracted pole Synthesis 22

2.4 Transformation to Band pass filter 27

3. Ku Bandpass Filter design **34**

3.1 Analysis of the selected topology 35

3.2 Layout generation 53

3.2 Ku Band Filter Model B 64

4. Sensitivity **68**

4.1 Worst Case Analysis 68

4.2 Sensitivity comparison between our filter vs Interdigital filter 72

5. Manufacturing and measurement **74**

5.1 Model A 75

5.2 Model B 77

5.3 Comparison of Various Coupled Line Tx-Filters 79

6. Conclusions and further work **80**

7. Bibliography **82**

List of Figures

Figure 1. Doubly terminated lossless transmission network. 15
Figure 2. Two-port network configuration 18
Figure 3. Nodal representation of a double loaded extracted pole filter with order N = 5 and two finite transmission zeros 23
Figure 4. Network topology considering the first node a NRN with dangling resonator 25
Figure 5. Remaining network to be extracted where the first element after an admittance inverter J is a NRN with dangling resonator 26
Figure 6. Network topology considering the last node a NRN with dangling resonator 27
Figure 7. Inline topology base don NRN dangling resonators 28
Figure 8. a) NRN dangling resonator with input admittances b) equivalent circuit for a resonator and a NRN. 28
Figure 9. a) Admittances circuit based on the input admittance of an NRN with dangling resonator. b) Equivalent circuit with distributed components (transmission's lines). 29
Figure 10. Schematic for a Nth-order fully extracted-pole filter by cascading N shunt open-short ended subs equivalent to the nodal topology in Figure 7, extracted from [9] 30
Figure 11. Schematic of (a) symmetric grounded coupled line together with two shunt open-end stubs. (b) Its equivalent circuit that is constituted by a J-inverter, two shunt open-ended stubs, and another two short-ended stubs at both the sides. [9]. 31
Figure 12. Equivalent circuits of Figure 11(b). (a) Each stub decomposed into two stubs. (b) Based on J inverter [16]. 32
Figure 13. NRN with dangling resonator topology of order 6 35
Figure 14. Low-pass filter response for 6 order filter based on the specifications 38
Figure 15. Ideal Schematic with short-ended and open-ended stubs 39
Figure 16. Circuit model S-parameters with (a) initial parameter values and (b) adjusted parameter values. 39
Figure 17. Layout of (a) stripline (b) microstrip transmission line format. Image extracted from [19] 42
Figure 18. Schematic based on coupled lines and ideal ground planes 44
Figure 19. Circuit model S-parameters of the solution obtained through optimization 45
Figure 20. Microstrip via-hole ground (a) ideal circuit (b) equivalent circuit with losses 46

Figure 21. Microstrip shorted-stub with via-hole (a) geometry (b) mounted circuits on aluminum fixtures and SMA connectors for measurement. Pictures extracted from [22] 47
Figure 22. Simulated (redstar) and measured (bluecircles) magnitude of reflection parameters |S11| and transmission parameters |S21| of microstrip shorted stub shorted with a 400μm diameter via-hole. Pictures extracted from [22] 47
Figure 23. Via-hole ground dimensions (mm) 48
Figure 24. Ideal ground plane (purple), via-hole schematic model (blue) and via-hole ground EM model (red) impedances on a Smith Chart 49
Figure 25. Schematic based on coupled lines with via-hole ground 50
Figure 26. Circuit model S-parameters of the coupled lines with via-hole ground solution obtained through optimization..... 51
Figure 27. Response comparison between coupled line with ideal ground planes schematic (red and dark blue traces) and coupled line with via-hole ground schematic (purple and loose blue dash traces)..... 52
Figure 28. Schematic of the first coupled line section and two open-ended stubs..... 53
Figure 29. a) Initial layout b) layout component c) final layout of the first coupled line section and two open-ended stubs 54
Figure 30. a) S11 b) S22 schematic impedance (blue) and initial layout impedance (red) on a smith chart..... 54
Figure 31. a) Return losses and Transmission losses b) phase for the schematic (dashed lines) and the initial layout (solid line)..... 55
Figure 32. a) S11 b) S22 schematic impedance (blue) and tuned layout impedance (red) on a smith chart..... 56
Figure 33. a) Return losses and Transmission losses b) phase for the schematic (dashed lines) and the tuned layout (solid line). 56
Figure 34. Schematic based on coupled lines with via-hole ground with the first coupled line section and the two open-ended stubs substituted by the layout component 56
Figure 35. Schematic of the second coupled line section and one open-ended stubs..... 57
Figure 36. a) S11 b) S22 schematic impedance (blue) and tuned layout impedance (red) on a smith chart..... 57
Figure 37. a) Return losses and Transmission losses b) phase for the schematic (dashed lines) and the tuned layout (solid line). 58
Figure 38 a) Initial layout b) layout component c) final layout of the second coupled line section and one open-ended stub..... 58

Figure 39. Schematic of the third coupled line section 59
Figure 40 a) Initial layout b) layout component c) final layout of the third coupled line section 59
Figure 41. Layout of the filter in Momentum 60
Figure 42. Final Layout in 3D of the filter version A in HFSS 61
Figure 43. Final Response of the filter A 62
Figure 44. Schematic based on coupled lines with via-hole ground with a capacitance of value 0.5fF between input and output 62
Figure 45. Circuit model S-parameters of filter A (a) Nominal and (b) with an extra capacitance of 0.7fF between the input and the output 63
Figure 46 Schematic based on coupled lines with via-hole ground Model B 65
Figure 47. Circuit model S-parameters of the coupled lines with via-hole ground model B solution obtained through optimization 65
Figure 48. Final Layout in 3D of the filter version B in HFSS 66
Figure 49 Final Response of the filter B 66
Figure 50. WCA width for the filter A 68
Figure 51. WCA width for the filter B 69
Figure 52. Via- hole position deviation on the X and Y axes 69
Figure 53. WCA via-hole position for the filter A 70
Figure 54. WCA via-hole position for the filter B 70
Figure 55. WCA extreme case of width and via-hole position for the filter A 71
Figure 56. Interdigital filter of order 6 72
Figure 57. WCA via-hole position for Interdigital filter of order 6 72
Figure 58. Comparative graph between the deviation of the via-holes in our filter and an interdigital filter 73
Figure 59. Probe station to measure the substrates with pico probes 74
Figure 60. Agilent PNA-X N5242A 74
Figure 61. a) CS-2-150 pico probes b) Calibration substrate for CS-2-150 75
Figure 62. Filter model A 75
Figure 63. Measured response of the filter A 76
Figure 64. Filter model B 77
Figure 65. Measured response of the filter B 77
Figure 66. Measured response of the filter B (solid lines) vs simulated response with the corrections in table 19 (dashed lines). 78

List of Tables

Table 1. Multiplication of *P(s)* by j to satisfy orthogonality condition. 19
Table 2. Filter specifications 34
Table 3. Filter specifications modified with extra margin 36
Table 4. Transmission zeros in w-plane and f-plane 37
Table 5 Short-ended and open-ended stubs impedance for 6 order filter 38
Table 6. Short-ended and open-ended stubs impedance for 6 order filter after tuning 38
Table 7. Parameter comparison between different types of substrate 40
Table 8. Comparison between Microstrip and Stripline transmission lines..... 42
Table 9. Design rules for Alumina substrate with AFT/TFP manufacturer..... 43
Table 10. Dimensions of the Coupled lines with ideal ground planes and the open-ended stubs optimized..... 44
Table 11. Dimensions of the Coupled lines with via-hole ground and the open-ended stubs optimized..... 50
Table 12. Parameter comparison between ideal and real schematic..... 52
Table 13. Dimensions of the first coupled line section and the two open-ended stubs 57
Table 14. Dimensions of the second coupled line section and the open-ended stub..... 58
Table 15. Dimensions of the third coupled line section..... 59
Table 16. Final Dimensions of the filter A 63
Table 17. Comparison between ideal schematic, real schematic and final Layout model A. ... 64
Table 18. Parameter comparison between ideal schematic, real schematic, final layout model A and final layout model B..... 67
Table 19. Nominal values vs manufactured values 78
Table 20. Comparison of Ku Band filters realized on Alumina substrate 79
Table 21. Statement of compliance for filter model B..... 80

1. Introduction

In the world of radiofrequency and microwaves, we now more often focus on making higher frequency designs due to the increase on bandwidth that we can use on communications and the reduction in size and mass of devices and designs.

In particular in this thesis the frequency range that we will focus on will be from 12.7 GHz to 14.7 GHz, the Ku Band Uplink. This band is mainly used for satellite communications, like the broadcasting services. So this kind of communication requires a receiver which is composed by an antenna, that catches the signal, an amplifier to increase the level of the signal and a filter to reject the non-desired frequencies like the spurious generated by the LNA or mixer.

The planar technology is mainly used for the design of the filters in aerospace communications due to the benefits which provides such as small size of the layouts, the compatibility with the other stages of the devices, the little weight of the equips and the cost.

The most used filter topologies with planar technology for the Ku band are the coupled line filter [1] [2], hairpin filter [2] [3], and interdigital filter [2] [4]. The first two have the advantage of achieving a good electrical performance but their physical dimensions are usually large. The third one has lower dimensions but the electrical performance is greatly affected by the manufacturing tolerances and even more affected when we work at higher frequencies.

Some of the topologies designed with planar technology, for example the interdigital filter, require using via holes in order to create a path from a conductive layer to a ground plane. The problem comes in the process of manufacturing because the positioning tolerances of the via-hole ground can change significantly the electrical length of the resonator altering the response of the filter. The other manufacturing tolerances are not as critical compared to those of the via-holes ground since the via-hole tolerances are 17 times higher than any other. In addition, these effects on the tolerances are more noticeable as we increase the frequency as the dimensions of the equipment are significantly smaller.

To reduce the affectation of the positioning tolerances of the via-hole ground it will be used a topology based on non-resonator nodes with dangling resonator and the use of the general extracted pole method to design the filter. The reason is that this topology allows us to generate transmissions zeros that are independent from the rest of the resonators and the coupled sections are also independent. These properties make choosing this topology a good choice to reduce the filter sensitivity.

Therefore, the objectives of the thesis are to design a Ku Band filter based on planar technology with the extracted pole method by using a NRN with dangling resonator topology, carry out a full-wave simulation in order to learn and evaluate the affectations and the effects of the different parameters in the filter and evaluate whether or not this topology is more robust.

Finally, manufacture a prototype and measure it to verify that it complies with the self-imposed specifications and correlate the measurements with the full-wave simulations.

With this, we aim to familiarize ourselves with the design process carried out; from the structure of the study through the design on the simulation software's (Matlab, ADS, Momentum and HFSS), the manufacture of the prototype and its measurement with the corresponding equipment, as in our case a probe station connected to a network analyzer

2. Filter Theory

This chapter will be focused on explaining most of the theory used along the thesis. It will be presenting the main characteristics of the Lossless Low pass prototype Filter Functions, the synthesis process for the characteristics polynomials to realize a Chebyshev prototype filter, the polynomials forms of the transfer and reflection parameters and the general extracted pole synthesis used in the design of the filter. In the last part of the chapter the steps to follow up to the transformation from the low pass prototype to Band pass filter will be shown.

2.1 Characterization of Lossless Low pass prototype Filter Functions

A filter network is an elemental component on any communication system that allows transmitting and attenuating signals in certain frequency bands. The synthesis of filter networks is carried out by designing a linear network prototype. That is, a lumped lossless low pass filter normalized in frequency, impedance, and terminated with resistors of equal value.

The Figure 1 is a general representation of a doubly terminated network capable of maximum power transfer.

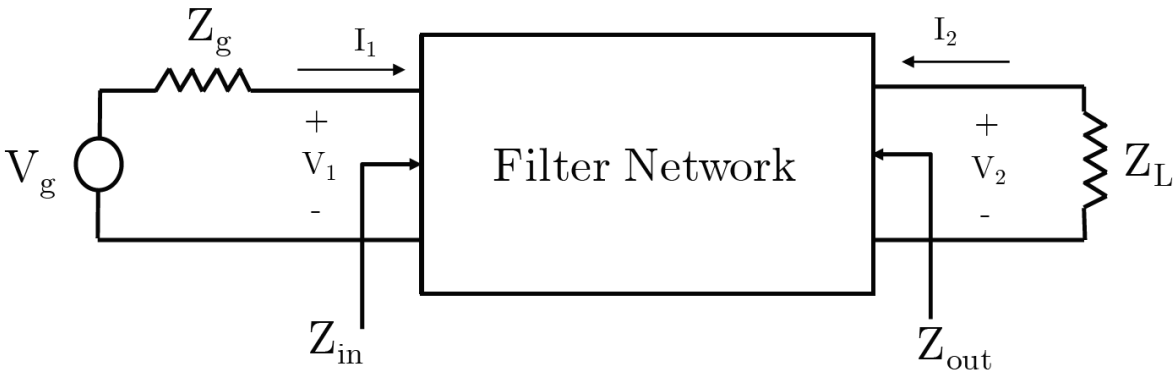

Figure 1. Doubly terminated lossless transmission network.

The reflection coefficient ρ for a two ports network is defined as the ratio of incident and reflected wave

$$\rho = \pm \frac{reflected\ wave}{incident\ wave} \tag{1}$$

Where the positive sign is used when the ratio is defined in terms of voltages while the negative one is used to define the ratio in terms of current waves. The reflection coefficient can be defined as

$$|\rho(j\omega)|^2 = \frac{reflected\ power}{available\ power} = \frac{P_r}{P_{max}} \tag{2}$$

The reflected power plus the transmitted power delivered to a load must equal the available power as

$$\frac{reflected\ power}{available\ power} + \frac{transmitted\ power}{available\ power} = 1$$

$$|\rho(j\omega)|^2 + |t(j\omega)|^2 = 1 \tag{3}$$

Where $t(j\omega)$ is defined as the transmission coefficient and represents the ratio of the transmitted wave to the incident wave.

We can relate the reflection coefficient ρ for a two port network from the transmission line theory [5] as

$$\rho(s) = \frac{Z_{in}(s) - R_1}{Z_{in}(s) + R_1} = \frac{z_{in}(s) - 1}{z_{in}(s) + 1}; \qquad z_{in}(s) = \frac{z_{in}(s)}{R_1} \tag{4}$$

The input impedance is a positive function and it can be defined as:

$$z(s) = \frac{n(s)}{d(s)} \tag{5}$$

It is a normalized impedance where $n(s)$ and $d(s)$are the numerator and denominator polynomials. Then

$$\rho(s) = \frac{z(s)-1}{z(s)+1} = \frac{n(s)-d(s)}{n(s)+d(s)} = \frac{F(s)}{E(s)} \tag{6}$$

We can conclude that [7]:

1. The denominator polynomial $n(s) + d(s) = E(s)$ must be the Hurwitz polynomial, with all its roots lying inside the left half of the s-plane.

2. The numerator polynomial $n(s) - d(s) = F(s$ may or may not be Hurwitz polynomial. However, the polynomial coefficient must be real and, as a result, its roots must be real or at the origin or occur in conjugate complex pairs.

So the magnitude of ρ is given by:

$$|\rho(j\omega)|^2 = \frac{F(s)F^*(s)}{E(s)E^*(s)} \tag{7}$$

For $s = j\omega$ we have:

$$\begin{gathered} |\rho(j\omega)|^2 = \frac{F(s)F(-s)}{E(s)E(-s)} \\ |t(j\omega)|^2 = \frac{E(s)E(-s)-F(s)F(-s)}{E(s)E(-s)} = \frac{P(s)P(-s)}{E(s)E(-s)} \end{gathered} \tag{8}$$

Polynomials $E(s)$ and $F(s)$ are normalized to ensure that the transmitted power is equal to or less than the available power. The three polynomials *E(s)*, *F(s)*, and *P(s)* are known as characteristic polynomials. The properties for the low pass prototype filter networks can be summarized as follows [6]:

F(s) is a polynomial with real coefficients, and its roots lie along the imaginary axis as conjugate pairs where the degree is N (order of the filter). *F(s)* can have multiple roots only at the origin. The roots represent frequencies at which no power is reflected (reflection zeros). At these frequencies, the filter loss is zero, and *F(s)* is pure odd or even polynomial.

P(s) is pure even polynomial with real coefficients. Its roots lie on the imaginary axis in conjugate pairs. Such roots represent frequencies at which no power is transmitted, and the filter loss is infinite (transmission zeros). Its roots can also occur as conjugate pairs on the real axis or as a complex quad in the s-plane. The roots' degree is ≤ n, where n is the order of the filter

E(s) is a strict Hurwitz polynomial, as all its roots lie in the left half of the s-plane where the degree is N.

So, in terms of characteristic polynomials

$$S_{11}(s) = \frac{F(s)}{E(s)};\ S_{21}(s) = \frac{P(s)}{E(s)} \tag{9}$$

2.2 Synthesis of a Generalized Chebyshev Filtering Function

Once the three characteristic polynomials are defined it is possible to relate them with a two port network configured as Figure 2.

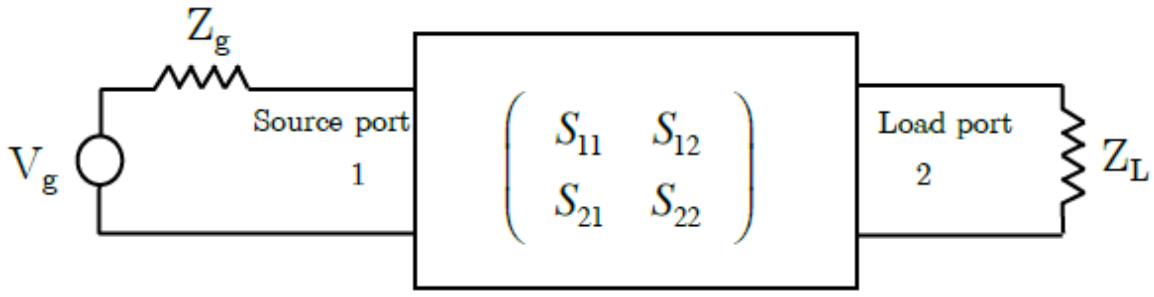

Figure 2. Two-port network configuration

So, the signal is transmitted from the source to the load port, obtaining the scattering matrix as:

$$\begin{pmatrix} b_1 \\ b_2 \end{pmatrix} = \begin{pmatrix} S_{11} & S_{12} \\ S_{21} & S_{22} \end{pmatrix} \begin{pmatrix} a_1 \\ a_2 \end{pmatrix} \tag{10}$$

Where b_1 and b_2 are the power waves propagating out of the circuit and a_1 and a_2 are the power waves propagating into circuit. Taking into account the energy conservation law equations for a passive, lossless and reciprocal network and the unique orthogonality equation [8], the reflection parameter S_{11} and the transfer parameter S_{12} can be related with the characteristics polynomials as

$$S_{11}(s) = \frac{F(s)/\epsilon_r}{E(s)} \rightarrow \begin{cases} F(s) = f_0 + f_1 s + f_2 s^2 + \cdots + F_N S^N \\ E(s) = e_0 + e_1 s + e_2 s^2 + \cdots + e_N S^N \end{cases}$$

$$S_{21}(s) = \frac{F(s)/\epsilon}{E(s)} \rightarrow \begin{cases} F(s) = f_0 + f_1 s + f_2 s^2 + \cdots + F_N S^{n_{tz}} \\ E(s) = e_0 + e_1 s + e_2 s^2 + \cdots + e_N S^N \end{cases} \quad (11)$$

2.2.1 Determination the P(s) polynomial

The polynomial *P(s)* is directly defined from the transmission zeros, t_z, since they are the roots of the polynomial. The transmission zeros are selected based on the filter specifications.

Depending on the number of resonators and transmission zeros, the polynomial *P(s)* must be multiplied by j in order to accomplish with the orthogonality condition as seen in Table 1. In this specific work, the filter is fully-canonical, that is N-n_{tz} even.

Table 1. Multiplication of *P(s)* by j to satisfy orthogonality condition.

N	**n_{tz}**	**(N-n_{tz})**	**Multiply P(s) by j**
Odd	Odd	Even	Yes
Odd	Even	Odd	No
Even	Odd	Odd	No
Even	Even	Even	Yes

2.2.2 Determination the F(s) polynomial

To calculate this polynomial a recursive method has to be used. The objective of the recursive method is to find the following expression:

$$Num[C_N(\omega)] = \frac{1}{2}[G_N(\omega) + G'_N(\omega)] \tag{12}$$

Such numerator corresponds to the F(w) polynomial.
After some mathematical development, it can be found that [7]:

$$U_i(\omega) = \omega U_{i-1}(\omega) - \frac{U_{i-1}}{\omega_i} + \omega' \sqrt{1 - \frac{1}{\omega_i^2}} V_{i-1}(\omega) \tag{13}$$

Where $\omega_i$correspond to the transmission zeros frequencies.

Now applying equation 15 and with some mathematics we can demonstrate that the numerator of $C_N(\omega)$ is equal to $U_N(\omega)$ after (N-1) cycles of this recursive method. Now, the zeros of $F(\omega)$ are revealed by finding roots of $U_N(\omega)$. As before we have to multiply by j to change from w plane to s plane and then the $F(s)$ coefficients can be found.

The next step is obtain the constants ϵ and ϵ_r and then determine the polynomial $E(s)$

2.2.3 Obtaining the constants ε and εr

As we said in a previous section the constants ϵ and ϵ_r are used to normalize $P(s)$ and $F(s)$ so $|S_{11}|$ and $|S_{21}|$ are < 1 for any value of s.

After some demonstrations [7], we know that for the fully canonical case ($N = n_{tz}$), where the highest degree coefficients are equal to unity, we can obtain

$$\frac{1}{\epsilon_r^2}+\frac{1}{\epsilon}=1 \rightarrow \epsilon_r=\frac{\epsilon}{\sqrt{\epsilon^2-1}} \tag{14}$$

Also we can define the insertion loss and return loss at $j=\pm\infty$ as

$$\begin{aligned} S_{21}(j\infty)&=\frac{1}{\epsilon}=20\log\epsilon\ \ dB \\ S_{11}(j\infty)&=\frac{1}{\epsilon_r}=20\log\epsilon_r\ \ dB \end{aligned} \tag{15}$$

Another way to obtain ϵ is from this equation

$$\epsilon=\frac{1}{\sqrt{10^{\frac{RL}{10}}-1}}\left|\frac{P(\omega)}{F(\omega)/\epsilon\_r}\right|_{\omega=\pm1} \tag{16}$$

2.2.4 Determination the $E(s)$ polynomial

Once we have $F(s), P(s)$ and the normalization constants, the $E(\omega)$ polynomial can be constructed using the following expression

$$E(\omega)=P(\omega)/\epsilon-jF(\omega)/\epsilon_r \tag{17}$$

The roots of the polynomial $E(\omega)$ have be conjugated in order to satisfy the Hurwitz condition.
After that, the $E(\omega)$ polynomial can be reconstructed and transformed to the *s* domain in order to obtain the $E(s)$ polynomial.

At this point, the characteristic polynomials are completely defined, so the transfer functions of the filter. The next step is to carry out the extraction procedure in order to obtain the Low pass prototype values of the network for such filter response

2.3 General extracted pole Synthesis

This method can be used for two-port networks which possess finite real frequency transmission zeros, where those are independently realized by separate interacting sections and it is very suitable for inline configurations as it is the case of the ladder-type filters.
With this method, a wide variety of prototype designed circuits can be derived depending on the elements in the nodal representation. The Figure 3 shows an example of a circuit with different types of extracted sections.

Basically, the sections will be extracted one by one using specific expressions based on the used topology which can be composed by four elements:

1) Resonators: These are represented by unit capacitances in parallel with frequency-independent reactance jb.
2) Admittance inverters: These are like the coupling coefficients between the nodes with a value J_i.
3) NRN: These are internal nodes that are connected to ground by frequency-independent reactances that mean a constant reactance jB_i.
4) The input (source) and the output (load): These are normalized conductances $G_s = G_L = 1$, for the case of no reactive ports.

Take into account that the building block that contains one dangling resonator coupled with a NRN generates one TZ at real frequency.

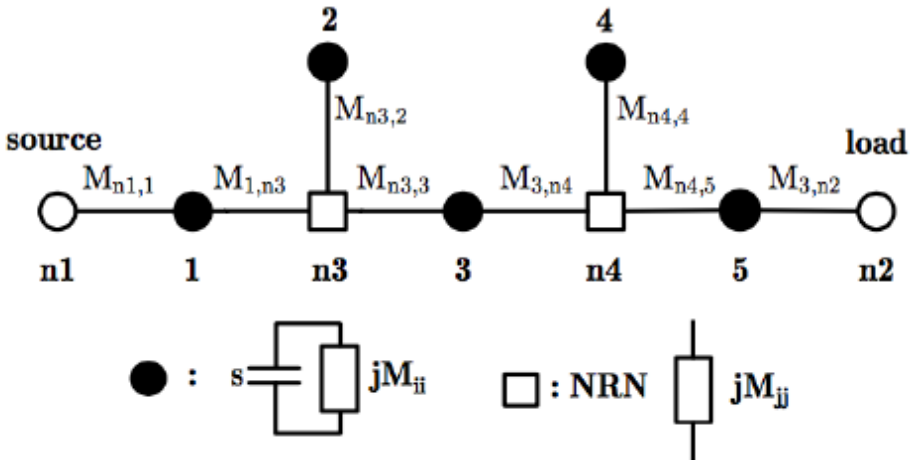

Figure 3. Nodal representation of a double loaded extracted pole filter with order N = 5 and two finite transmission zeros.

This approach to synthetize general inline prototypes of extracted pole filters describing general Chebyshev functions relies essentially on a Darlington technique [8]. In this theory only will be explained the cases for NRN with darling resonator.

2.3.1 Reflection coefficients S_{11} and S_{22}

In a lossless two-port network the input and output reflection coefficients, $S_{11} and\ S_{22}$ have the same poles as zeros. Can be expressed as follows:

$$S_{11}(s) = e^{j\theta_{11}}|S_{11}(\infty)|\frac{\prod_{i=1}^{i=N}(s-s_{zi})}{\prod_{i=1}^{i=N}(s-s_{pi})} = e^{j\theta_{11}}\frac{M(s)}{D(s)}$$
$$S_{22}(s) = e^{j\theta_{22}}|S_{22}(\infty)|\frac{\prod_{i=1}^{i=N}(s-s_{zi})}{\prod_{i=1}^{i=N}(s-s_{pi})} = e^{j\theta_{22}}\frac{M(s)}{D(s)} \quad (18)$$

Where S_{zi} and S_{pi} , i=1,2,…N, are the zeros and poles of S_{11} and S_{22}. The term $|S_{11}(\infty)|$ is only different to unit when n_{tz} =N, that will be our case. The phases $\theta_{11}\ and\ \theta_{22}$ have to be taken in consideration in the extraction process

It can be related the input reflection coefficient with the input/output admittance from the source to load. Then if we consider that the internal conductance of the source or load is normalized to the unity we have the next equations:

$$Y_{in}(s) = \frac{1 - S_{11}(s)}{1 + S_{11}(s)} = \frac{D(s) - e^{j\theta_{11}} M(s)}{D(s) + e^{j\theta_{11}} M(s)}$$
$$Y_{out}(s) = \frac{1 - S_{22}(s)}{1 + S_{22}(s)} = \frac{D(s) - e^{j\theta_{22}} M(s)}{D(s) + e^{j\theta_{22}} M(s)} \quad (19)$$

As it can be seen in the equation 24, the phase term modify the input and output admittance changing the extracted prototype network and the value of the input/output phase will be determined examining the behaviour of the input and output admittances of the circuit, which is used to implement the specified filter.

2.3.2 Extraction of First node NRN with dangling resonator

Considering that the first node is an NRN, of constant reactance jB, which is connected to a dangling resonator by an inverter J_2 like Figure 4 the phase of the reflection coefficient is obtained by evaluating the admittance asymptotically the input admittance which take the form

$$Y_{in}(s) = \frac{J_1^2}{jB + \frac{J_2^2}{s - jw_z} + \frac{J_3^2}{y'(s)}} \quad (20)$$

We can see that the input admittance has a zero at the position of the pole $s = j\omega_z$. Using this condition in 25, we have:

$$e^{j\theta_{11}} = \left.\frac{M(s)}{D(s)}\right|_{s=jw_z} = 1 \quad (21)$$

Similarly, if the first node from the output is a NRN connected to a dangling resonator, which generates poles in $s = j\omega_z'$, we get:

$$e^{j\theta_{22}} = \left.\frac{M(s)}{D(s)}\right|_{s=jw'_z} = 1 \quad (22)$$

With the reflection coefficients fully specified, we can determine the input and output admittance to start the extraction process with 24.

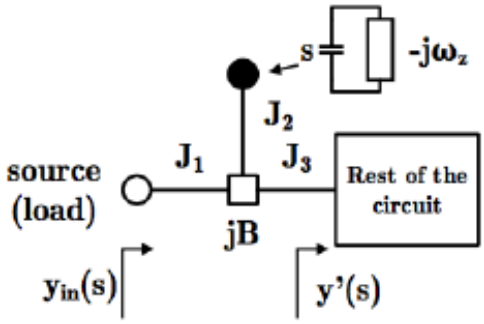

Figure 4. Network topology considering the first node a NRN with dangling resonator

2.3.3 Extraction of a NRN with Dangling resonator

Let us assume that, at a given cycle in the extraction process, the remaining circuit, as seen from the input (or the output), is of the form shown in Figure 5. The input admittance can be defined as

$$Y_{in}(s) = \frac{J^2}{\frac{J_1^2}{s - jw_z} + jB + y'(s)} \rightarrow \frac{J^2}{y_{in}(s)} = \frac{J_1^2}{s - jw_z} + jB + y'(s) \tag{23}$$

As we can note, we only can obtain the ratio of J and J_1. This is a very useful property of NRNs that allows multiple solutions for a given synthesis problem. A convenient solution would be to arbitrarily set J=1 and continue with the extraction. The equation (29) shows that J_1 is related to the residue of the left hand side at $s = j\omega_z$.

$$J_1^2 = J^2 residue \left(\frac{1}{y_{in}(s)}\right)\Big|_{s=jw_z} \tag{24}$$

Then the new admittance after the admittance inverter can be obtained as

$$Y_{in}^{n1}(s) = \frac{J^2}{y_{in}(s)} - \frac{J_1^2}{s - jw_z} = jB + y'(s) \tag{25}$$

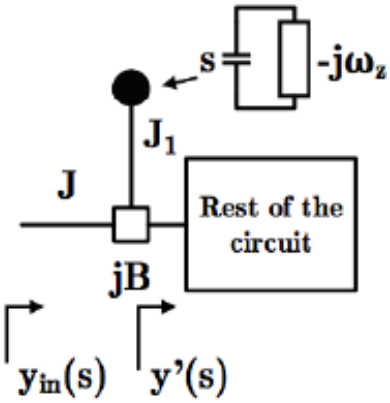

Figure 5. Remaining network to be extracted where the first element after an admittance inverter J is a NRN with dangling resonator

Again, to determine jB, we have to evaluate the admittance $Y_{in}^{n1}(s)$ at a zero of the admittance $y'(s)$. Considering only the case that the first node in $y'(s)$ is a NRN connected to a dangling resonator which generates a pole at $s = j\omega_z$, the $y'(s = j\omega_z) = 0$ and

$$\begin{aligned} B &= Im\left[Y_{in}^{n1}(s)\big|_{s=w_z}\right] \\ Y_{in}^{n2}(s) &= Y_{in}^{n1}(s) - jB \end{aligned} \tag{26}$$

This completes the extraction of the resonator leaving an input admittance again $y_{in}(s)$.

2.3.4 Extraction of Last Node NRN with dangling resonator

Although it is preferable to extract the elements of the network from the input and output simultaneously to minimize the effect of round off errors, for completeness, we give the equations to extract the last node of the circuit either starting from the input or the output.

Considering that the last node is a NRN with a dangling resonator, the remaining input admittance is of the form (Figure 6)

$$Y_{in}(s) = \frac{J^2}{\frac{J_1^2}{s - jw_z} + jB + \frac{J_2^2}{G_L}} \rightarrow \frac{J^2}{y_{in}(s)} = \frac{J_1^2}{s - jw_z} + jB + \frac{J_2^2}{G_L} \tag{27}$$

The next relation can be established from the admittance inverter J_1:

$$J_1^2 = J^2 residue \left(\frac{1}{y_{in}(s)}\right)\Big|_{s=jw_z} \tag{28}$$

Then, finally we have

$$\begin{aligned} B &= Im\left[\frac{1}{y_{in}(\infty)}\right] \\ J_2^2 &= J^2 Re\left[\frac{1}{y_{in}(\infty)}\right] \end{aligned} \tag{29}$$

Note that the value of J is arbitrary in this case.

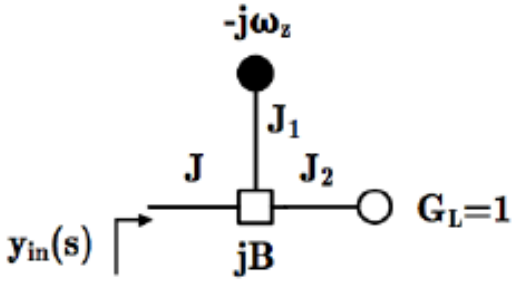

Figure 6. Network topology considering the last node a NRN with dangling resonator

2.4 Transformation to Band pass filter

Once we have all the elements of the selected topology we are able to transform these low pass elements into band pass filter. In order to do that it is necessary to select a technology, in this case it will be planar technology, and then we will be able to create a distributed model based on planar technology.

This section will be explained based on the topology selected for the design of the Ku band filter; more information related to other topologies in can be found in [9].

As we said, the topology selected will be an inline topology with NRN dangling resonators like Figure 7.

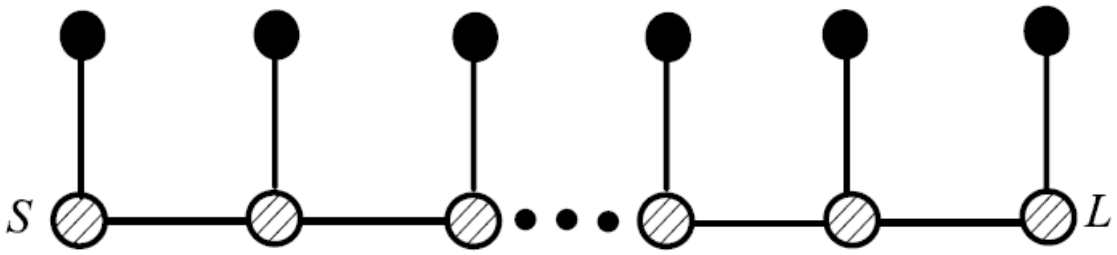

Figure 7. Inline topology base don NRN dangling resonators

First, it will be analysed the NRN with dangling resonator and then relate it with the distributed model for later prototyping.

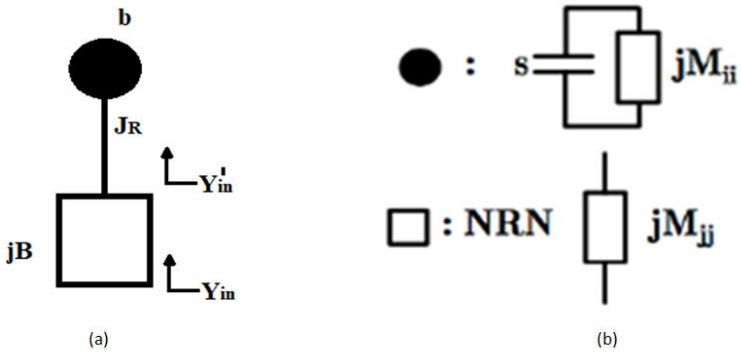

Figure 8. a) NRN dangling resonator with input admittances b) equivalent circuit for a resonator and a NRN.

It will be taken Figure 8(a) as reference for the development and the mathematics considering a NRN with dangling resonator node. So, as we can see in Figure 8(b) the resonator is equivalent to a capacitance, s, and a reactance, *jb*. Starting from that we can obtain the input admittance after the NRN as:

$$Y'_{in} = \frac{J_R^2}{s - jb} \tag{30}$$

Also we can determine the input admittance before the NRN

$$Y_{in} = jB + \frac{J_R^2}{s - jb} \tag{31}$$

Then we can relate this admittance to an equivalent distributed circuit as Figure 9.

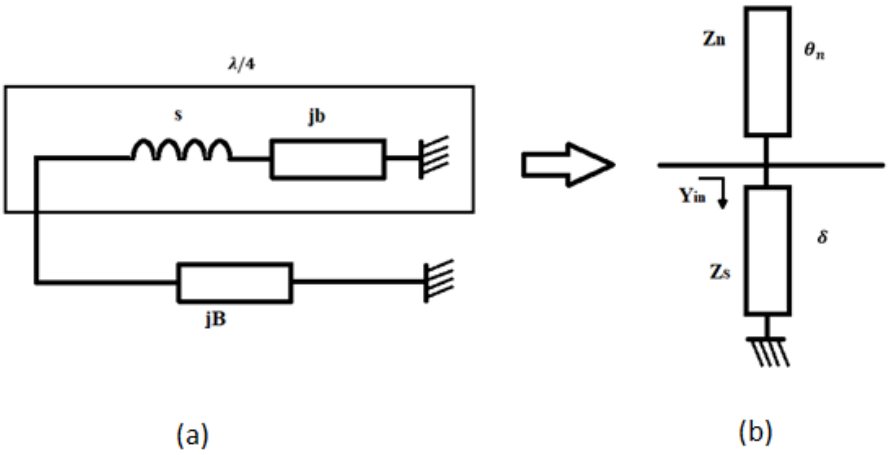

Figure 9. a) Admittances circuit based on the input admittance of an NRN with dangling resonator. b) Equivalent circuit with distributed components (transmission's lines).

Focusing on the Figure 9(b), there are two specific areas, one section is shunted with an open-ended stub and other one, a short-ended stub. So for the first situation, the open-ended stub is adjusted to provide a quarter wavelength (i.e., $\theta_n = \pi/2$) at the frequency of the transmission zero, f_z. The short-ended stub is related to the NRN with input admittance Y_{in}, and thus Figure 8(a) becomes exactly an extracted-pole section as Figure 9(b) generating the t_z at f_z. Note that the NRN appearance is based on the narrowband assumption, under which condition Y_{in} is reasonably considered as a frequency invariant constant.

Taking as reference Figure 8(a) and Figure 9(b) a fully extracted-pole Nth-order filter that performs either non canonical (i.e., $n_{tz} < N$) or fully canonical (i.e., $n_{tz} = N$) functions, centered at f_0 with a *Bw* bandwidth, is constructed conveniently by cascading N open-ended resonators, N short-ended resonator and a J_{pk} inverter. So the schematic proposed is like Figure 10.

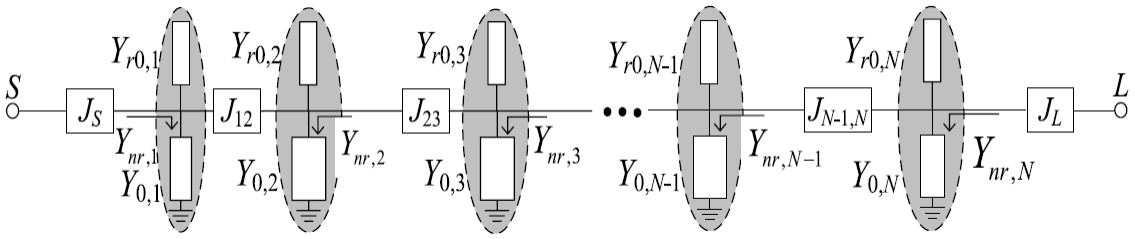

Figure 10. Schematic for a Nth-order fully extracted-pole filter by cascading N shunt open-short ended subs equivalent to the nodal topology in Figure 7, extracted from [9]

So, now the key point is to relate the extracted elements with the impedance of the open-ended and short-ended stubs and with de inverters J_{pk}. The way to calculate the impedances is starting from the general expression of the characteristic impedance.

$$Z_{in} = Z_0 \left[\frac{Z_A + jZ_0 \tan(\beta L)}{Z_0 + jZ_A \tan(\beta L)} \right] \tag{32}$$

Then in order to calculate a short circuit line we know that $Z_A = 0$ and then

$$Z_{sc} = jZ_0 \tan(\beta L) \tag{33}$$

And in the case of an open circuit line, $Z_A = \infty$ so we have

$$Z_{oc} = -jZ_0 \cot(\beta L) \tag{34}$$

With the equations 33 and the extracted elements, it can be related in the next form:

$$Z_{sc} = -\frac{Z_0}{\frac{B}{j} \cdot \tan(\beta L)} \tag{35}$$

And with the equation 34, the extracted elements and equalling the slope of the susceptance of the parameter B and the slope of the resonator [9] it can be obtained the next equation

$$Z_{oc} = \frac{4}{\pi} \cdot \frac{Z_0}{2} \cdot \frac{2 \cdot D + b_i}{J_{Pk}} \tag{36}$$

Where Z_0 is the characteristic impedance of a transmission line, normally 50 Ohms, D is the quotient between f_0, central frequency of the filter, and Bw ,the bandwidth; b_i are the transmission zeros, βL is the electrical length and B is the reactance of a NRN.

Now that all the values for the components of the circuit are found, it can be used a technique to compact a fully extracted pole filters by means of a novel structure, as Figure 11. It consists in use an asymmetric grounded coupled line with even/odd – mode characteristic admittances Y_e and Y_o, and electrical length θ together with two open-ended stubs, with characteristic admittances $Y_{r0,p}$ and $Y_{r0,k}$ and electrical lengths $\theta_{r,p}$ *and* $\theta_{r,k}$.

Based on the principle discussed in [10], the introduced circuit structure can be equivalent to a network that possesses a J -inverter, two shunt open-ended stubs and two short-ended stubs at both sides.

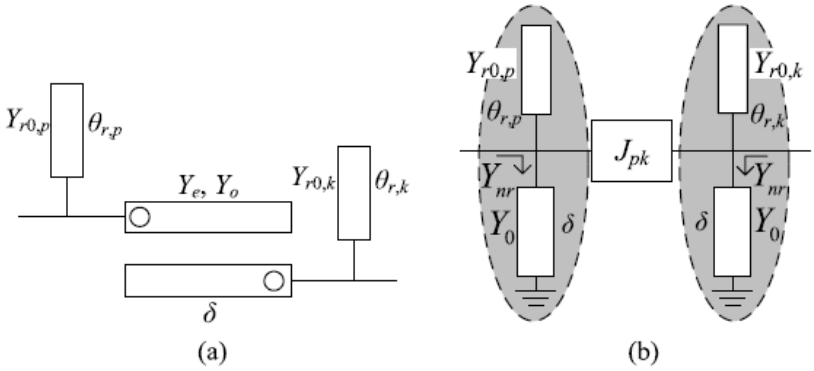

Figure 11. Schematic of (a) symmetric grounded coupled line together with two shunt open-end stubs. (b) Its equivalent circuit that is constituted by a J-inverter, two shunt open-ended stubs, and another two short-ended stubs at both the sides. [9].

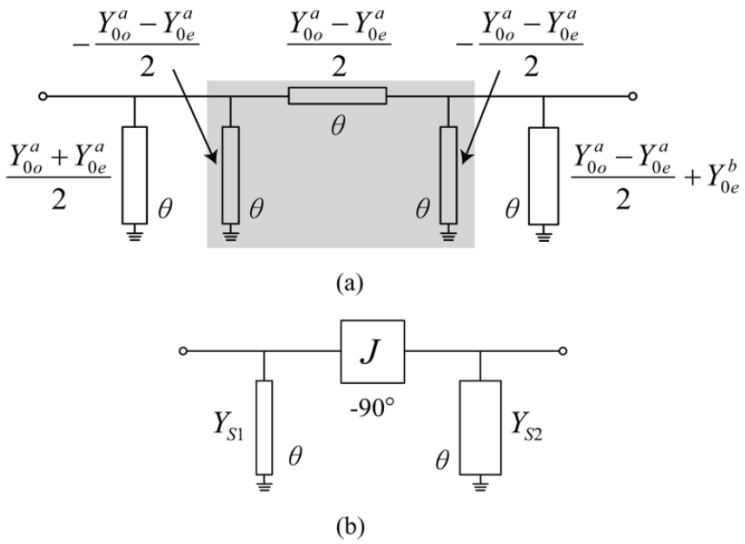

Figure 12. Equivalent circuits of Figure 11(b). (a) Each stub decomposed into two stubs. (b) Based on J inverter [16].

Figure. 11(a) shows the schematic of an asymmetric coupled line. An advantage of using asymmetric coupled lines instead of symmetric coupled lines is that the additional design parameter allows to perform complex functions. On the other hand, the proposed method utilizes asymmetric coupled lines whose equivalent circuit is a transmission-line section loaded with two different stubs, as shown in Figure 11(b).

Based on this equivalent circuit it can be seen that each stub in Figure 11(b) can be decomposed into two stubs, as in Figure 12(b) in which the shaded part is equivalent to a J inverter. Therefore, the asymmetric coupled-line section in Figure 11(a) can be modelled as a J inverter loaded with two different shunt stubs, as in Figure 12(b) where

$$\begin{aligned} J &= \frac{Y_{0_o}^{\ a} - Y_{0_e}^{\ a}}{2sin\theta} \\ Y_{S1} &= \frac{Y_{0_o}^{\ a} - Y_{0_e}^{\ a}}{2} \\ &= Y_{0_e}^{\ a} + Jsin\theta \\ &= Y_{0_o}^{\ a} - Jsin\theta \end{aligned} \tag{37}$$

And

$$\begin{aligned} Y_{S2} &= Y_{0_e}^{\ b} + \frac{Y_{0_o}^{\ a} - Y_{0_e}^{\ a}}{2} \\ &= Y_{0_o}^{\ b} + \frac{Y_{0_o}^{\ a} - Y_{0_e}^{\ a}}{2} \\ &= Y_{0_e}^{\ b} + Jsin\theta \\ &= Y_{0_o}^{\ b} - Jsin\theta \end{aligned} \tag{38}$$

Now, all the necessary parameters are found and the physical dimensions has to be calculated. There are several methods to obtain them like full-wave method [12], Green's function integral equation method [13], modal approach [14], [15], the approximate method based on the impedances and propagation constants of symmetric coupled lines [16], solve iteratively the equations in [10] or like in our case doing an optimization process starting from an initial seed next to the final solution.

This concludes the theory part. In the next chapter it will be explained step by step the design of a Ku filter using as reference the theory explained in this chapter.

3. Ku Bandpass Filter design

In this chapter it will be explained all the steps that have been made, from the synthesis explained on the previous chapter through the circuit distributed with ideal elements and with real elements based on the selected substrate to the final layout. Also it will be explained the choice of the nodal topology, the selected substrate and the different choices proposed in this design.

In order to properly design the Ku filter, the state of compliance must be specified. Our design will have to accomplish the following parameters:

Table 2. Filter specifications

PARAMETERS	VALUES	COMMENTS
Bandwidth	12.7-14.7 GHz	
Return Losses	≥15 dB	Value in the Frequency band
Rejection Bands	≥40dB at 9 GHz	
	≥40dB at 17 GHz	
Footprint (I ·L)	8x4mm	Maximum allowed area

Starting from Table 2, in the first section of the chapter it will be explained the nodal topology used, including the order of the filter, and it will be shown the resulting ideal schematic based on the impedances calculated according to the selected topology.

3.1 Analysis of the selected topology

The filter will be based on a Chebyshev topology, because we want to have transmission zeros at finite frequencies, making our filter more selective and: obtaining higher rejection bands values. Regarding to the reflection zeros, the position of them also will cause better response shape in the band of the filter.

The selected Chebyshev topology will be the following:

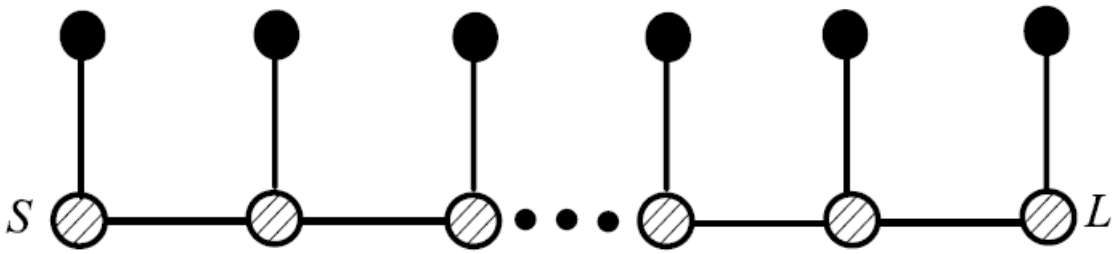

Figure 13. NRN with dangling resonator topology of order 6

This topology has been chosen because NRN with dangling resonator topology allowed us to generate transmissions zeros that are independent from the rest of the resonators. One more reason of this choice is that you can obtain the equivalent circuit with planar technology, and this technology help us to make the filter more compact as we will be seeing later.

The order of the filter will be 6, in order to accomplish the specifications of bandwidth and the rejection band values.
Now, we have to define the position of the transmission zeros, as we can see in Figure 13, n_{tz} = N, so we will have to define six transmission zeros. Once we have defined them, according to the specifications in Table 2, we are able to start the synthesis process of the filter.

Several points have been considered in order to improve the design and to anticipate possible manufacturing tolerances and/or deviation in the materials.

- The first one is related to the bandwidth, due to the sensitivity and tolerances in this range of frequency and the shape response a margin must be added to prevent possible frequency shifting, caused by the change of the substrate permittivity or the via tolerances.
- The second point is increasing the values of Return Losses and rejection bands to have a margin. This has been done in order to accomplish the specifications even though the manufacturing tolerances may deteriorate the response. Also because the schematic and the EM simulations will be different due to the parameters of dielectric and conductor materials, and especially in this range of frequency.

So, for our design and synthesis we have considered the following specifications:

Table 3. Filter specifications modified with extra margin

PARAMETERS	VALUES	COMMENTS
Bandwidth	12.5-14.5 GHz	400 MHz more
Return Losses	≥25 dB	10dB more
Rejection Bands	≥45dB at 9 GHz	5dB more
	≥45dB at 17 GHz	5dB more
Footprint (I ·L)	8x4mm	Maximum allowed area

Using Table 3, the synthesis process can start. In order to ease the design in later stages, like in the layout generation, it has been searched to have a symmetric topology, later it will be able to see the benefit to use this design note.

So taking into account all the information mentioned previously, it will be implemented the theory explained in Chapter 2 using a Matlab script with the necessary specifications from Table 3.

The transmission zeros lie in the ω plane because the synthesis starts from the low pass prototype form, in Table 4 it can be seen the t_z in the ω plane and in the f plane after the bandpass transformation:

Table 4. Transmission zeros in w-plane and f-plane

Transmission Zeros	
ω plane (rad/s)	f plane(GHz)
3.2	18
3.7	18.85
3.9	19.2
3.9	19.2
3.7	18.85
3.2	18

As we can see, the TZ have been selected first to comply the rejection levels in table 2 and second for accomplish the self-condition of being a symmetric topology.

Then, with the transmission zeros and Table 4 the characteristic polynomials can be found, section 2.1, with the obtained polynomials the extracted pole method, section 2.2, can be used to determine the elements of the topology in Figure 13. Figure 14 shows the low pass filter response obtained from the Matlab script and the specifications.

After the extraction of the elements of our topology, the transformation has to be done from the low pass to the Band pass filter. In order to do this transformation a technology has to be chosen, in our case the filter will be manufactured in planar technology.
The planar technology is the most used technology in the aerospace sector especially when working at high frequencies, but that is not the only reason, the planar technology allows us to obtain designs or circuits smaller and less heavy compared to other technologies such as cavity technology. Afterward, it will be presented which substrate and RF/microwave transmission-line format will be used.

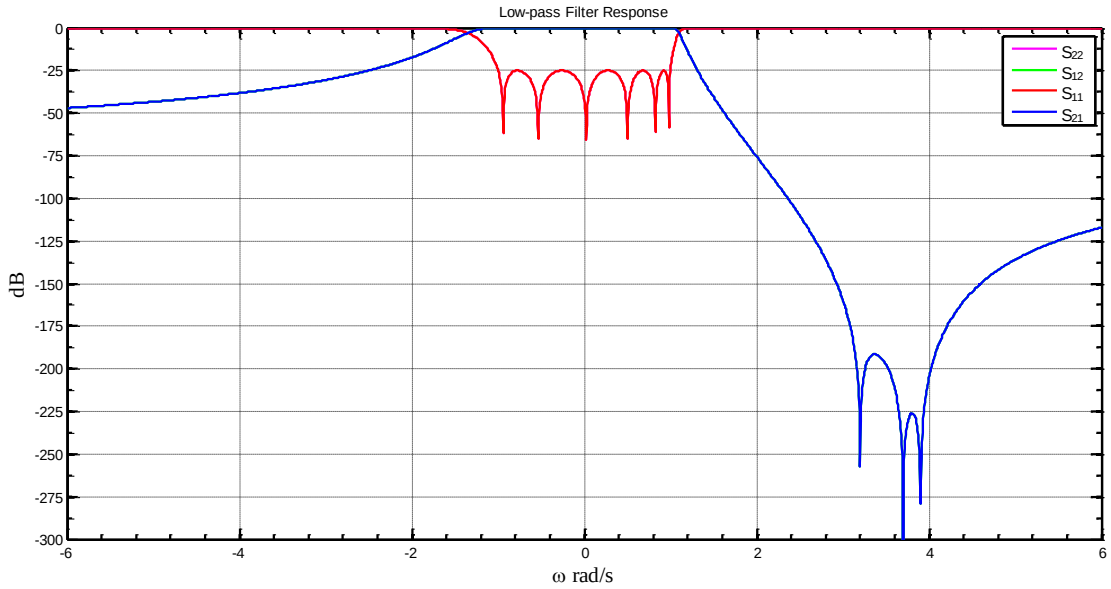

Figure 14. Low-pass filter response for 6 order filter based on the specifications

Now, with the extracted elements the transformation to bandpass can be performed, applying the equations 41-42 the resulting impedances are the following:

Table 5 Short-ended and open-ended stubs impedance for 6 order filter

n	**1**	**2**	**3**	**4**	**5**	**6**
Z_{sn} (Ω)	103.51	41.18	29.25	30.05	39.95	105.75
Z_{nn} (Ω)	86.7	44.35	33.5	34.45	42.55	85.65

The impedance Z_s corresponds to the open-ended stub, where the phase, θ_s is $\pi/2$ and the Z_n is the impedance related to the short-ended stub, where the phase θ_n allows a degree of freedom, in our case $\pi/6$.

So, with the obtained impedance and the chosen phases we can generate the schematic and simulate it to have an experimental verification. The filter is simulated by using ADS 2015 version.

Table 6. Short-ended and open-ended stubs impedance for 6 order filter after tuning

n	**1**	**2**	**3**	**4**	**5**	**6**
Z_{sn} (Ω)	95.8	39	29.1	29.1	39	95.78
Z_{nn} (Ω)	86.7	42.9	35	35	42.9	86.7

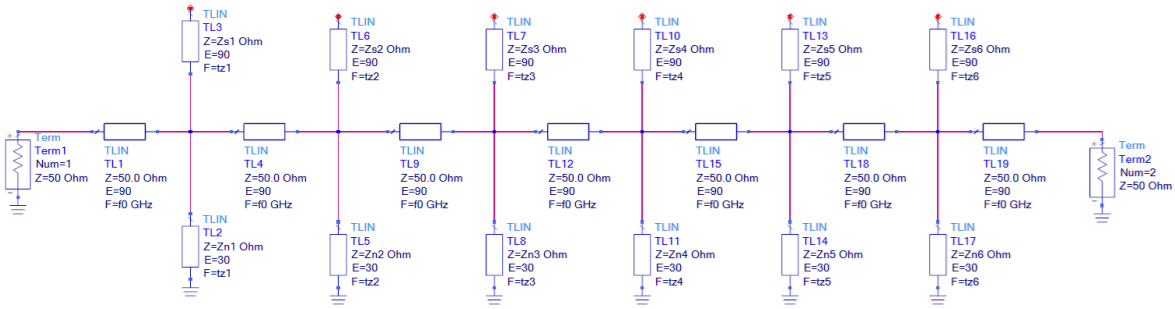

Figure 15. Ideal Schematic with short-ended and open-ended stubs

We can see the resulting schematic in Figure 15 note that the transmission lines of 50 Ohms impedance and 90 degree phase corresponds to the J inverter from Figure 10 or Figure 12. The chosen value for the J inverter is 1, in order to do easier the design and the mathematic developments.

The initial circuit model response is shown in Figure 16(a). Since the extracted-pole sections are equivalently realized here, the expressions used are theoretical approaches that are also used for narrow bandwidths, besides that the wavelength is so small that doing any little change to the impedance may cause larges mismatches in the final response, it is reasonable that slight adjustments may be required for the circuit parameters. Take into account that the first and last resonators are those that are the most sensitive and can cause more changes to a filter response. The final circuit model response, after the tuning, is illustrated in Figure 16(b). The adjusted parameters can be found in Table 6.

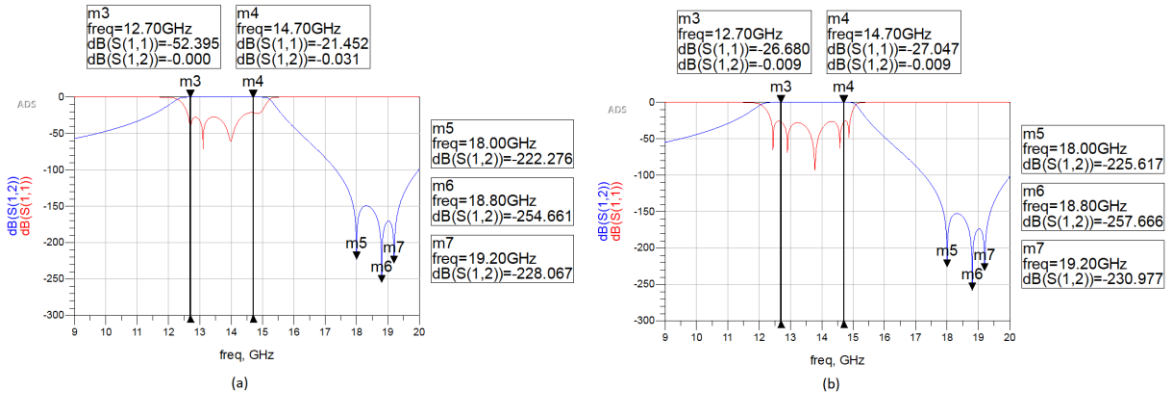

Figure 16. Circuit model S-parameters with (a) initial parameter values and (b) adjusted parameter values.

As we can see in Figure 16(b) the filter design accomplishes all the electrical parameters. The transmission zeros, makers 5, 6 and 7, are in the chosen frequency, 18GHz, 18.85GHz and 19.2GHz. The return losses in the specified bandwidth and the rejection band levels at 9GHz and 18GHz also fulfil the specifications. The problem will appear when calculating the physical dimensions, as the dimensions of the filter will be too large; therefore the specifications of Table 2 will not be accomplished. To check the problem is enough to calculate the filter dimensions just basing in the dielectric permittivity without choosing any type of material yet. So if we calculate the dimensions by choosing a high dielectric permittivity like 10, it will show us that this topology does not accomplish the specification of envelope.

To solve this issue, it will be used the theory in 2.4 to transform two short-ended stubs with a J inverter (50 ohms transmission line with 90 phase) in to asymmetric coupled lines (Figure 12). Because the ADS does not have asymmetric coupled transmissions lines (ideal form) it will be necessary to go directly to distributed model considering final physical dimensions. So, first a dielectric substrate and RF/microwave transmission-line format have to be chosen. Apart from that, depending on the substrate the manufacturer rules [18] have to be taken into account when designing the filter.

The substrate will be Alumina, in particular Alumina A493 from Kyocera. Normally, in the aerospace sector there are two mainly substrates that are being used, Duroid and Alumina. In the following table the characteristics of various materials are summarized:

Table 7. Parameter comparison between different types of substrate

Parameters	**A493**	**Duroid 6002**	**TMM10i**
Dielectric constant	9.6	2.94	9.8
Loss tangent	0.0002	0.0012	0.002
Thermal conductivity(W/mK)	26	0.6	0.76
Coefficient thermal expansion	7.2	16	20
Conductor Material	Gold	Copper	Copper
Conductor conductivity (σ)	4.1e7	5.8e7	5.8e7

In Table 7, it can be seen some differences between the substrates. The main differences are the losses; the loss tangent and the conductor conductivity are lower than other substrate used normally. Another point is the parameters related to the temperature which as you can see the Thermal conductivity is very high compared to the Rogers substrate, this means that the design response will change much less depending on the temperature than the Roger substrates. This is a key point in the aerospace sector because the equips usually works in a temperature range from -55 to 65 ºC, so the less the response changes depending on the temperature, the better it will be controlled the design. Other important parameter is the size and is directly related to the dielectric constant, so the smaller the dielectric constant, the greater the design size.

Apart from the parameters in Table 7, the range of frequencies where you want to work also matters in the selection of the substrate. That is because when you work at low a frequency the performance for Rogers substrate can be enough or as good as could be in Alumina and this translate into less cost. Also it must be taken into account other points. For example, the maximum or minimum substrate size will limit what kind of substrate can be used; this means that depending on the frequency range we will use one or the other. Also, as we commented previously, the manufacturing resolution allows us to make the manufactured design similar to the simulated one; in this case, the resolution for the Alumina substrate is more accurate, so at high frequencies, where the wavelength is so small that any small change in the design will modify the response, the Alumina is the best substrate to use. Last but not least, the cost, the Alumina substrates cost two or three times more than the Rogers, the reason is that the Alumina is basically a ceramic material which the different manufacturing processes and the conductor make it more expensive.

So based on what we stated before, the substrate has to be Alumina for the following reasons:

- The high range frequency
- The manufacturing resolution needed to fabricate the filter.
- The losses have to be as small as possible.
- The compactness and the size of the filter
-

The format of the transmission line will be microstrip. Then it will be explained each format of transmissions lines and the main differences between them.

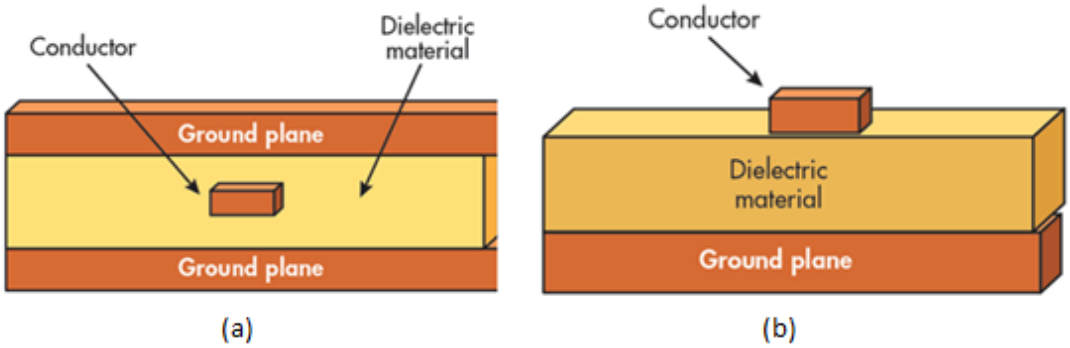

Figure 17. Layout of (a) stripline (b) microstrip transmission line format. Image extracted from [19]

The stripline incorporates top and bottom ground planes with dielectric insulator material surrounding a center conductor in a balanced configuration.

The Microstrip is a relatively simple circuit configuration with top conductor, dielectric layer, and bottom ground plane. It is easy to manufacture and place components.

The following table summarize shows the differences between microstrip and stripline

Table 8. Comparison between Microstrip and Stripline transmission lines

Features	**Microstrip**	**Stripline**
Structure	Conducting layer, dielectric layer and ground layer	Top and bottom ground plane, dielectric layer, embedded conducting layer within dielectric
Characteristic impedance	20 to 120 Ohm	35 to 250 Ohm
Width of line at same impedance	Wider	Narrower
Manufacturing tolerances	Tighter	Lighter
Radiation Loss	High for low ε and Low for high ε	Low
Dielectric Loss	Less	More

Dispersion	Low	None
Advantages	• Smaller size • Easy to fabricate • Easy to troubleshoot	• Good EM shielding can be achieved with this structure • Low attenuation loss • Wider bandwidth • Better isolation
Disadvantages	• Unwanted radiation in uncovered microstrip based configuration • Higher loss • Poor isolation among adjacent lines	• Complex and expensive in fabricating it. • Stripline Trace width is smaller compare to microstrip line of same impedance and height. • Tuning or troubleshooting is complex.

So based on Table 8 and as we said before the microstrip will be format of the transmission line on our design.

Then the design will be done with Alumina A493 with microstrip lines. Before moving to the design with the substrate, it is necessary to know the design rules of this material. In Table 9 are shown the parameters to keep in mind.

Table 9. Design rules for Alumina substrate with AFT/TFP manufacturer

Distance	**Size**	
	Standard	**Minimum**
Conductor/Conductor (µm)	≥20	≥10
Conductor line width (µm)	≥20	≥10
Conductor parallel to substrate edge (µm)	≥50	
Via diameter (d) (µm)	≥300	≥150
Conductor width of vias (µm)	≥150+d	≥100+d

Now, all the required information is known and the final schematic can be generated. To do that the physical dimensions must be found. Applying the equations in 43-44, it is possible to obtain the admittances even and odd for each transmission line. After that, to obtain the physical dimensions a process of optimization will be done, as we said in 2.4.

The process of optimization is performed by means of Advanced Design System (ADS) software. To perform that, the microstrip circuit has to be set up to be optimized (Figure 18). As we said before the substrate will be Alumina, the substrate thickness will be 10 mils (0.254mm) and the conductor thickness, gold, will be 3µm.

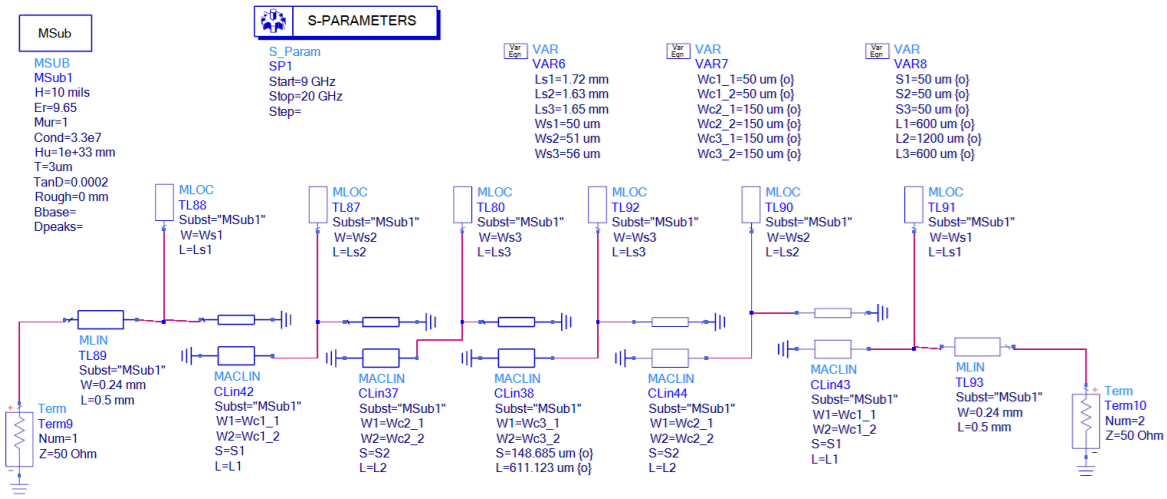

Figure 18. Schematic based on coupled lines and ideal ground planes

After an adjustment of the dimensions, the asymmetric lines are characterized with the following parameters:

Table 10. Dimensions of the Coupled lines with ideal ground planes and the open-ended stubs optimized

	$MCLIN_1$	**$MCLIN_2$**	**$MCLIN_3$**	**$MCLIN_4$**	**$MCLIN_5$**
W_CL_1 (mm)	65.5	166.5	146.75	166.5	65.5
W_CL_2 (mm)	65.75	178.5	146.8	178.5	65.75
Gap (S) (µm)	79.5	25	148.5	25	79.5
Length (L) (µm)	575	2200	615	2200	575

	$MLOC_1$	**$MLOC_2$**	**$MLOC_3$**
W_s (µm)	50	51	56
Length stub (L_s) (mm)	1.72	1.62	1.65

In this optimization process, we limit the minimum values of lines widths and the gap of the coupled lines to accomplish the standard design rules from Table 9. In the case of the stubs, an optimization is not necessary since the stubs have to keep the dimensions obtained through the Linecalc with the impedances of Table 6.

If we focus on the S parameters, Figure 19 shows a response that meets all the requirements on Table 3. Also the response is quite similar to the previous topology, the non-compact one, Figure 16(b) .The zeros are kept in the same frequencies where we have designed them, except for small displacements of just 20MHz.

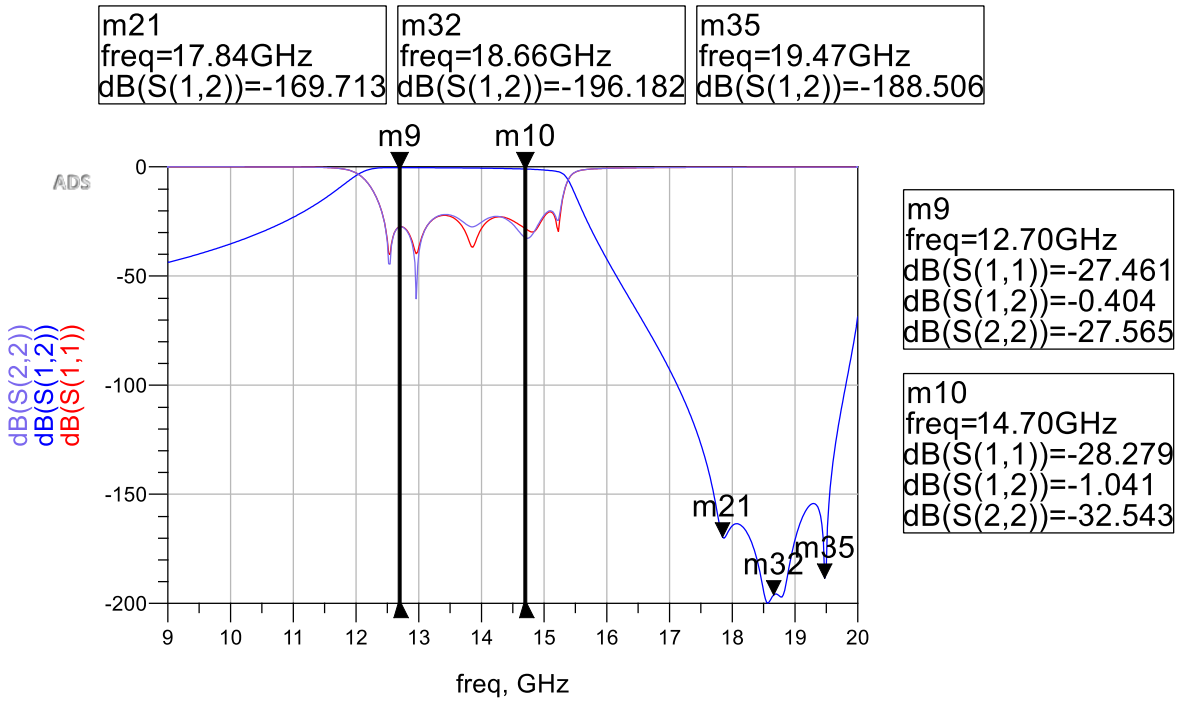

Figure 19. Circuit model S-parameters of the solution obtained through optimization

The optimization has been done considering ideal grounds but in the final layout in order to connect the conductive line with the ground plane has to be done by using via holes. The model of microstrip via-hole ground have a big affectation in the layout and the response of the filter, so big that once chosen the via hole model it will be necessary to be optimized again. So, before moving to the layout stage, it will be analyzed the via hole effect, it will be compared with the different ADS schematic models and we will re-optimize it with the via hole selected to get a schematic model as real as possible and thus facilitate the generation of the layout.

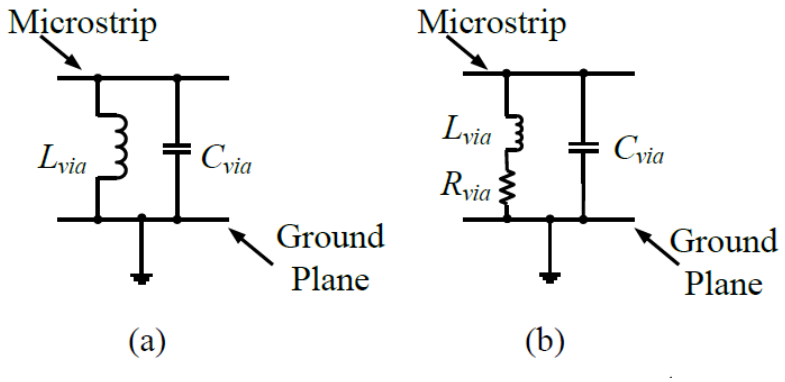

Figure 20. Microstrip via-hole ground (a) ideal circuit (b) equivalent circuit with losses

In the microstrip line, via-hole can be modelled by a series of inductance and resistance in parallel with the capacitance of the pad obtaining wideband short circuits.

The equivalent circuit of via-hole is shown in Figure 20(a) with no losses, Figure 20(b) including losses. According to [20] the inductance (L_{via}), resistance (R_{via}), of the microstrip via-hole can be calculated as below:

$$L_{via} = \frac{\mu_0}{2\pi} \cdot \left[h \cdot \ln\left(\frac{h + \sqrt{r^2 + h^2}}{r} \right) + \frac{3}{2} \cdot \left(r - \sqrt{r^2 + h^2} \right) \right] \tag{39}$$

The inductance is in picohenries (*pH*), h = length of via (substrate height) in µm, $r = D/2$ outer radius of via in µm, $\mu 0$ = free space permeability which is equals to 1.25664x10^{-6} H/m

$$R_{via} = R_{dc} \sqrt{1 + \frac{f}{f_\delta}} \tag{40}$$

where

$$R_{dc} = \frac{h}{\{\sigma[r^2 - (r-t)^2]\}} \tag{41}$$

and

$$f_\delta = \frac{1}{\pi \mu_0 \sigma t^2} \tag{42}$$

f = operating frequency, ζ = conductivity of the conducting material used for via, t = metal thickness, $f\delta$ = skin effect corner frequency

While the capacitance (C_{via}) which is the pad capacitance of the microstrip via-hole can be calculated as below [21]:

$$C_{via} = \frac{1.41\epsilon_r t d_1}{d_2 - d_1} \tag{43}$$

d_1= via-pad diameter, d_2= anti-pad diameter, t= thickness of dielectric material, ε_r= relative dielectric constant of the substrate

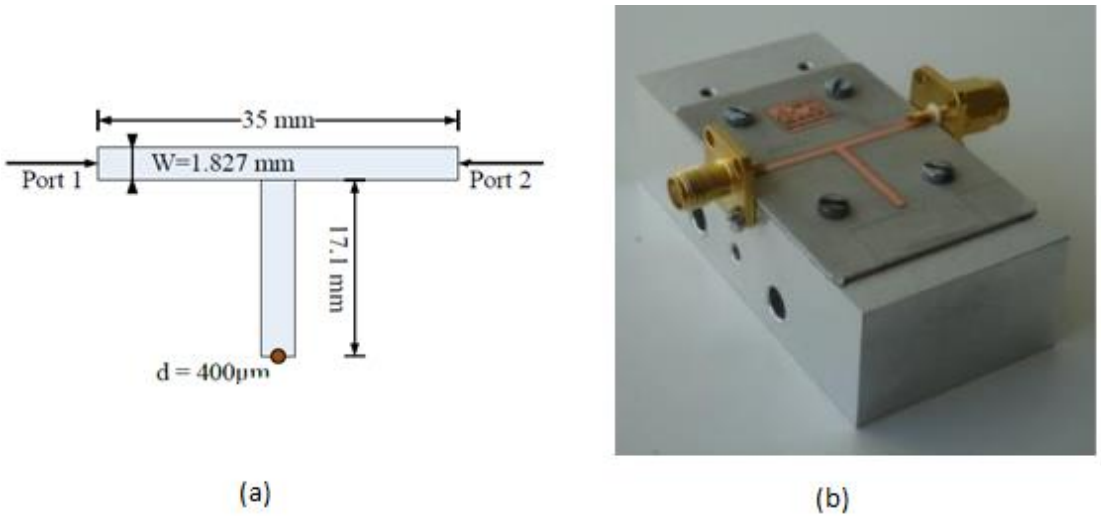

Figure 21. Microstrip shorted-stub with via-hole (a) geometry (b) mounted circuits on aluminum fixtures and SMA connectors for measurement. Pictures extracted from [22]

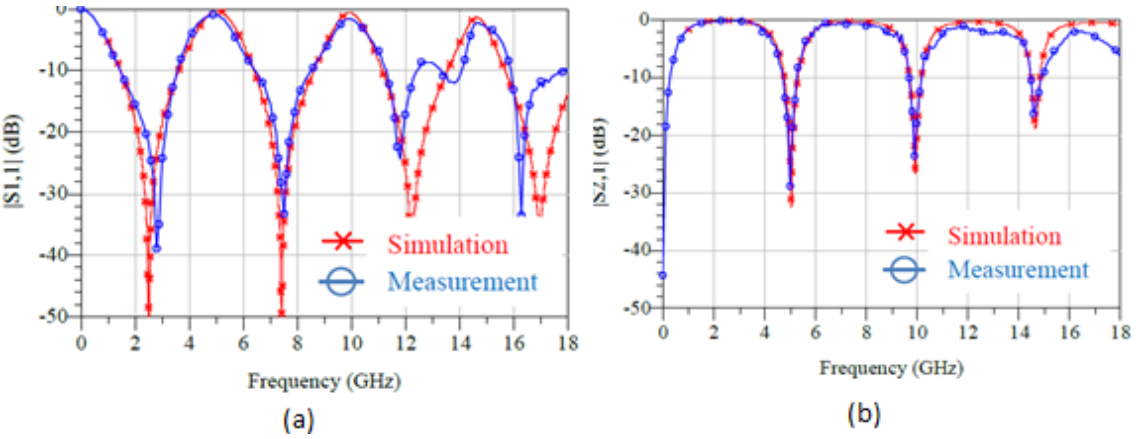

Figure 22. Simulated (redstar) and measured (bluecircles) magnitude of reflection parameters |S11| and transmission parameters |S21| of microstrip shorted stub shorted with a 400µm diameter via-hole. Pictures extracted from [22]

Figure 21 and Figure 22 show a shorted-stub microstrip with via-hole geometry and the performance in function of the frequency. It can be observed that when working at higher frequencies the via-hole ground ceases to resemble the model of the equations used. Also the manufacturing tolerances are more relevant at high frequencies than low frequencies also this can cause the change of the response. Anyway, the manufacturing tolerances are the biggest inconvenience for the filters at high frequencies and later it will be explained in more detail the problems related to via-hole grounds and the manufacturing tolerances.

The dimensions of the via-hole ground (Figure 23) have been chosen using the minimum dimensions from Table 9 to obtain a more compact design.

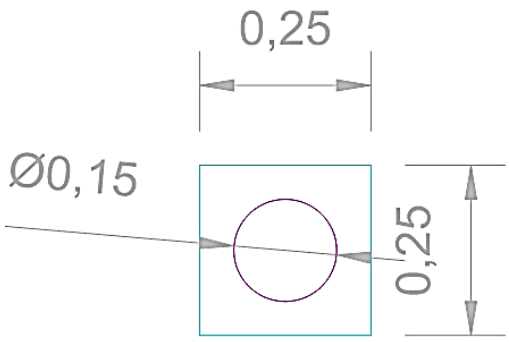

Figure 23. Via-hole ground dimensions (mm)

If we plot the impedance of the via-hole ground in the smith chart and we compare it with the ideal ground and the schematic via-hole ground impedances, we will be able to see the differences in the behaviour of those elements.

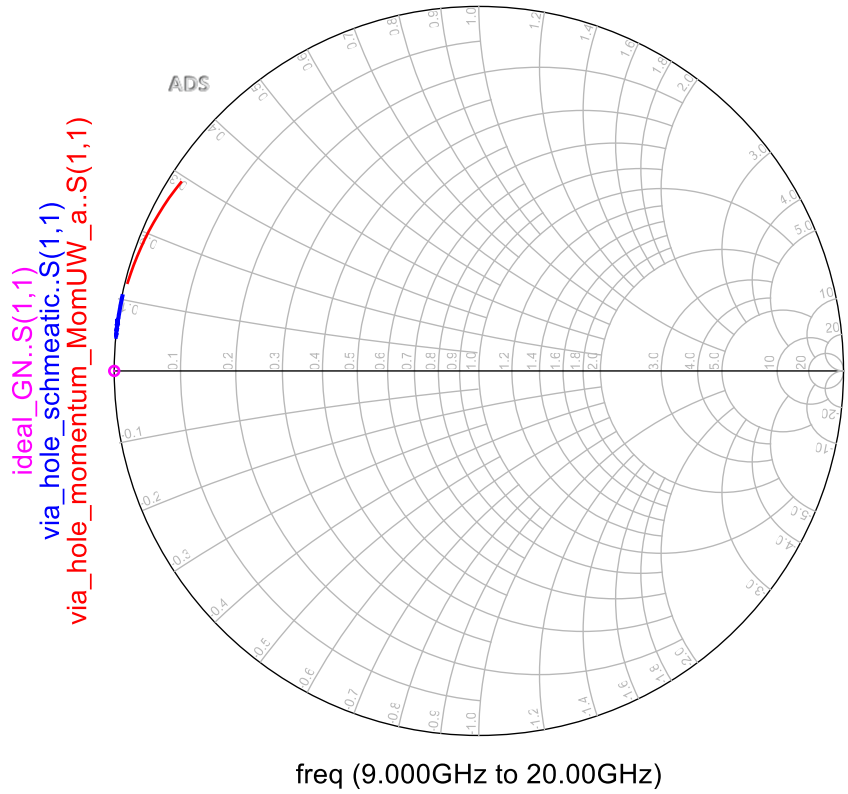

Figure 24. Ideal ground plane (purple), via-hole schematic model (blue) and via-hole ground EM model (red) impedances on a Smith Chart

As we can see in Figure 24, the via-hole ground momentum that is the real one, has a behaviour more inductive and resistive than the via-hole ground from the schematic. And obviously the impedance of the via-hole ground from momentum does not look like the ideal ground, that's why it is necessary to carry out a fine adjustment considering the via-hole from momentum.

So we will use the same method and the same goals in the optimization process that before. The circuit generated is shown in Figure 25. As we can see, the ideal ground plane has been replaced by the via-hole ground model simulated in momentum.

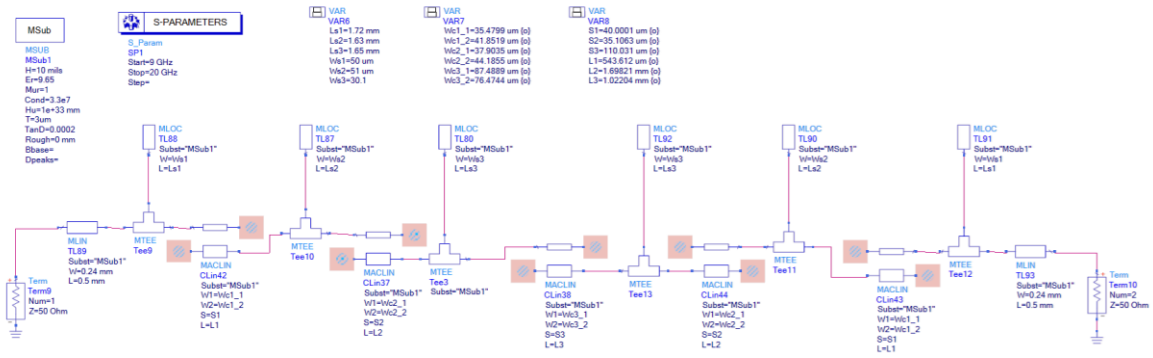

Figure 25. Schematic based on coupled lines with via-hole ground

The final dimensions are quite different to the ones with ideal ground plane (Table 11), as we saw before this is caused by the via-hole ground. On the one hand the inductance, resistance and capacitance introduced by the via-hole has to be compensated changing the widths, lengths and the separation of the asymmetric coupled lines, on the other hand the size of the pad and the via-hole add an extra electric length so in order to correct this, the asymmetric coupled lines has to be shortened. Regarding to the dimensions of the stubs (MLOC), also can be modified in order to correct this effects, but always keeping the position of the transmission zeros.

Table 11. Dimensions of the Coupled lines with via-hole ground and the open-ended stubs optimized

	$MCLIN_1$	**$MCLIN_2$**	**$MCLIN_3$**	**$MCLIN_4$**	**$MCLIN_5$**
W_CL_1 (µm)	35.5	38	87.5	38	35.5
W_CL_2 (µm)	41.8	44.2	76.5	44.2	41.8
Gap (S) (µm)	40	35	110	35	40
Length (L) (µm)	545	1700	1000	1700	545

	$MLOC_1$	**$MLOC_2$**	**$MLOC_3$**
W_s (µm)	30	110	20
Length stub (L_s) (mm)	1.72	1.63	1.65

Figure 26 shows the final response of the filter after the optimization with the via-hole ground model.

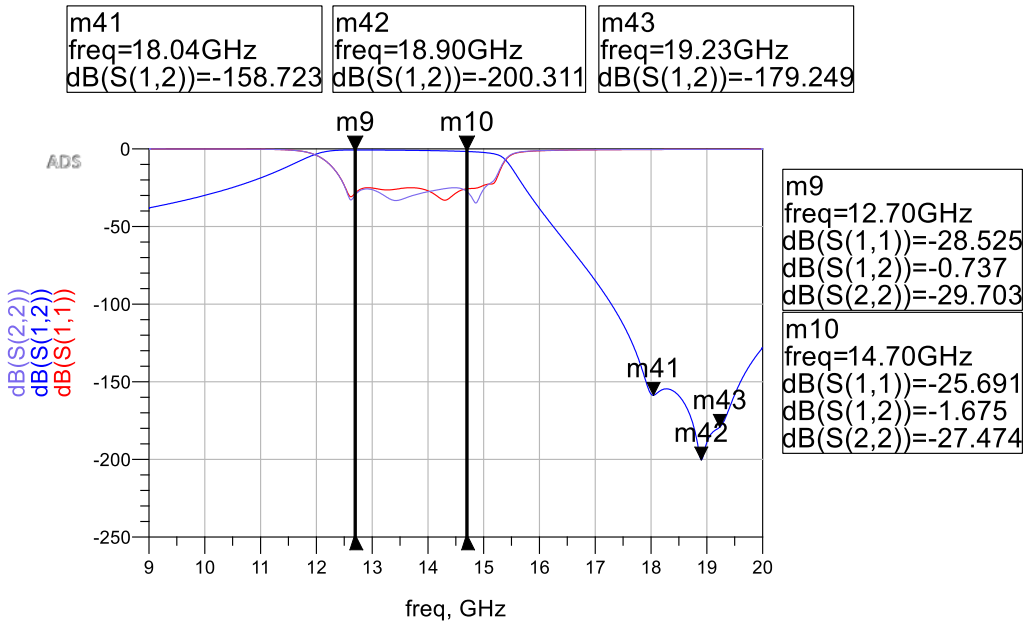

Figure 26. Circuit model S-parameters of the coupled lines with via-hole ground solution obtained through optimization

As we can see, the response is quite similar to Figure 19 where ideal ground planes were used instead of via-hole. The most relevant difference in the three models seen until now is the transmission response (S(1,2)) because as you can see in Figure 16, Figure 19, Figure 26 the losses are increasing, even more after adding the via-hole, but apart from this, having zeros of transmission in the upper band, on the one hand we make the filter more selective and increase the rejection band level but on the other hand we are creating a slope in the transmission band of the filter that causes an unbalance in the amplitude. As an example, in Figure 26, the marker 9, which corresponds to the low band part (12.7GHz), we got 0.7dB and in the marker 10, high band part (14.7GHz), we got 1.675dB, this means that we have an unbalance amplitude of approximately 1dB.

Before moving onto the next section, it will be compared the ideal schematic with the real one, in order to see the differences more easily and check that we meet the requirements of Table 3. So in Figure 27 we can see the plots comparing the responses of the ideal and real schematics.

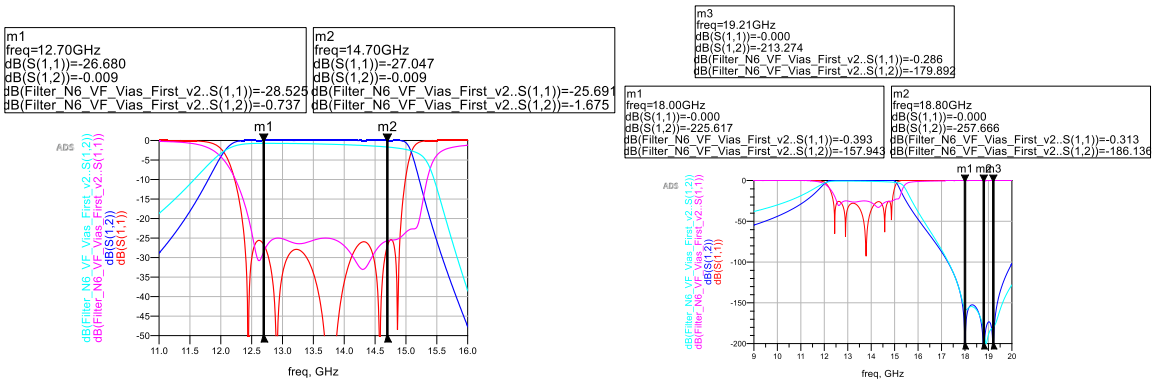

Figure 27. Response comparison between coupled line with ideal ground planes schematic (red and dark blue traces) and coupled line with via-hole ground schematic (purple and loose blue dash traces).

In Figure 27 it can be seen more clearly what has been said above about the transmission response and the position of the transmission zeros. Another difference is the reflection zeros, where in the ideal response the zeros can be seen more defined, this is because there are some effects that in the ideal schematic are not taken into account and this allows us to reach the points very close to the center of the smith chart. Some of the effects are due to the substrate, but the biggest affectation is caused by the via-hole ground, this can be easily corroborated, because in Figure 19, where we have used ideal ground planes, the reflection zeros are very similar to the ideal ones.

In the following table we have a small comparison of results between the ideal and the real schematic:

Table 12. Parameter comparison between ideal and real schematic.

PARAMETERS	IDEAL SCHEMATIC	REAL SCHEMATIC
Return losses	>26dB	>25dB
Insertion losses	<0.1dB	<1.7dB
Rejection Bands	>50dB at 9 GHz	>40dB at 9 GHz
	>100dB at 17 GHz	>100dB at 17 GHz

3.2 Layout generation

In this section will be explained the steps we have to follow to obtain the final layout from the schematic in Figure 25. Also it will be shown the simulated results and the comparison between the ideal and the schematic ones.

The first stage of de layout design will be done in ADS Momentum and the second one will be done in HFSS. The first stage consists in generating the different coupled sections separately, trying to obtain the same performance as the schematic section, and once we have them all, it can be put together and obtain the complete layout and the full response of the filter. The second stage consists in exporting the resulting layout from the first stage to HFSS and adjusting it to obtain the best performance possible.

The main differences between momentum and HFSS come from how the responses are calculated. On the one hand, momentum uses an infinite ground plane, the calculations are made with the surface currents and using theoretical approximations. On the other hand, HFSS is a 3D simulator which uses the fields to calculate the response, whether it is in a very precise way. It is more precise because for example it takes into account all the effects of the walls of the cavity and the effects of using a connector in case it is necessary

Having said that, we can being with the first stage, in order to do that we will focus on the first coupled line section and the two open-ended stubs that are next (Figure 28)

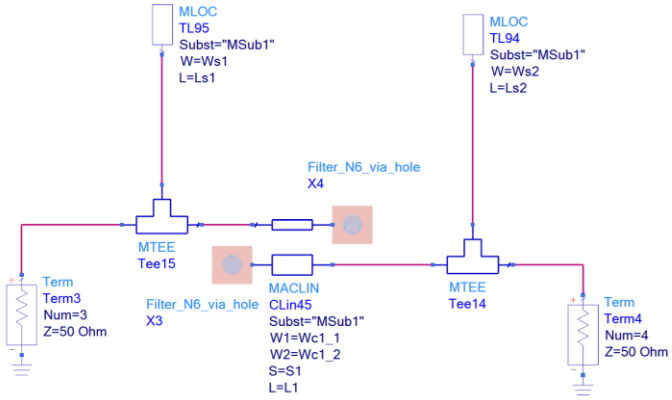

Figure 28. Schematic of the first coupled line section and two open-ended stubs

Next step is to generate the layout of this section with the physical dimensions obtained in Table 11. Dimensions of the Coupled lines with via-hole ground and the open-ended stubs optimized and simulate it. Then, the way to proceed is to compare the differents response, above all focus on the smith chart, between the schematic results and the layout results.

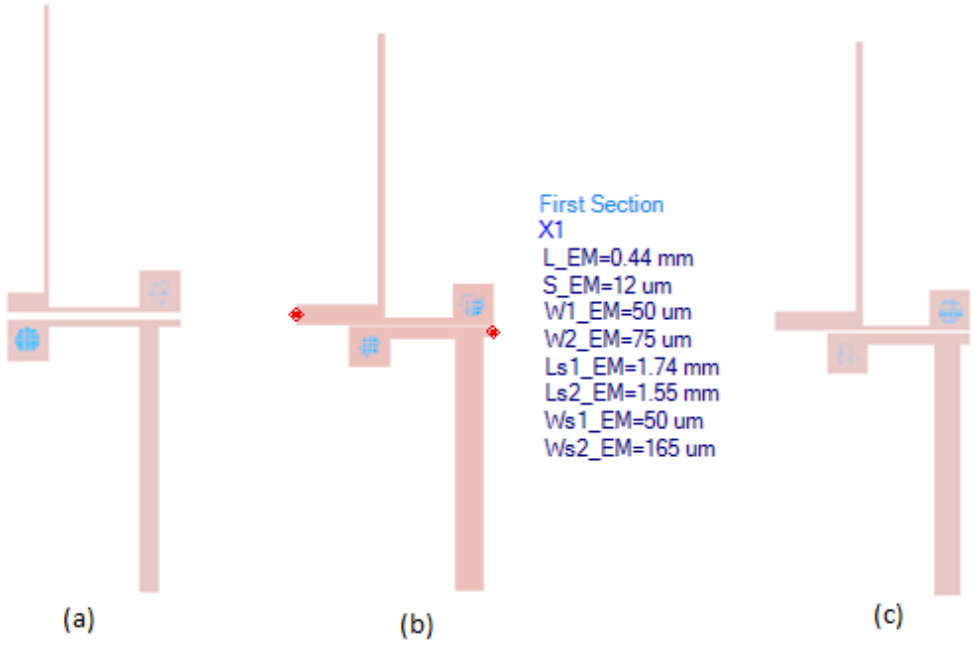

Figure 29. a) Initial layout b) layout component c) final layout of the first coupled line section and two open-ended stubs

Then with the layout generated from the schematic dimensions(Figure 29(a)), we can plot the different responses as follows:

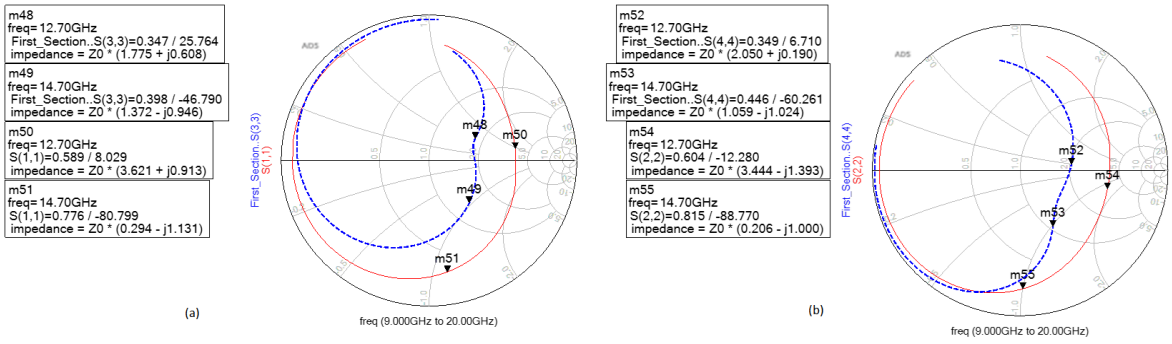

Figure 30. a) S11 b) S22 schematic impedance (blue) and initial layout impedance (red) on a smith chart.

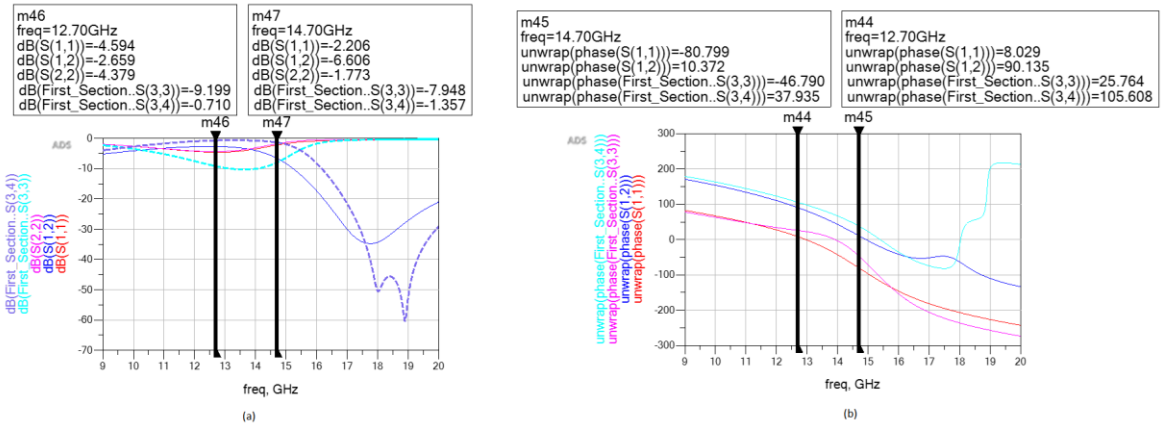

Figure 31. a) Return losses and Transmission losses b) phase for the schematic (dashed lines) and the initial layout (solid line).

As we can see in Figure 30 and Figure 31, the results corresponding to the layout coupled section are too different to the schematic ones, so we have to modify the layout to obtain the same results as the schematic. The main reasons that they do not coincide is due to the radiated fields and the couplings between the stubs, the coupled lines and the via-hole ground that cannot be taken into account in the schematics. And this type of effects, affect more the greater the frequency, in our design, the frequency is high enough to consider that this effects can change a lot the response as we have seen. Apart from that, the via-hole ground is the element on the structure that generates the couplings and radiated fields more undesired because cannot be considered a ground coupling as can be seen in the circuit of Figure 20.

To correct those effects the dimensions should be tuned. If we take as a reference the smith chart responses (Figure 30), we need to modify the red trace, both for $|S_{11}|$ and $|S_{22}|$, in order to obtain the blue trace. To do that, normally you start playing with the separation between the coupled lines or gap. In this case, we need to add capacity in order to move the response to the left, then by reducing the gap we increase the coupling, and this means that we add a capacity effect. The width of the coupled lines also helps to add an inductive or capacity effect. The length of the coupled lines has to be shortened or lengthened depending on the positions on the markers and how shifted the response is in function of the schematic response. Finally, it is necessary to tune the dimensions of the stubs, length and width, to center the response in the proper position. Normally, there is no order in which to make these modifications because every change can modify the response, so you have to tune it all together.

After tuning we obtain the following responses:

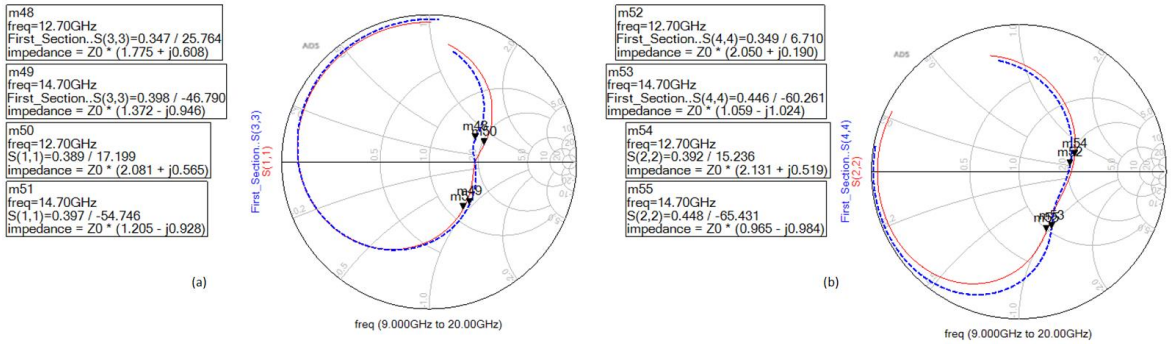

Figure 32. a) S11 b) S22 schematic impedance (blue) and tuned layout impedance (red) on a smith chart.

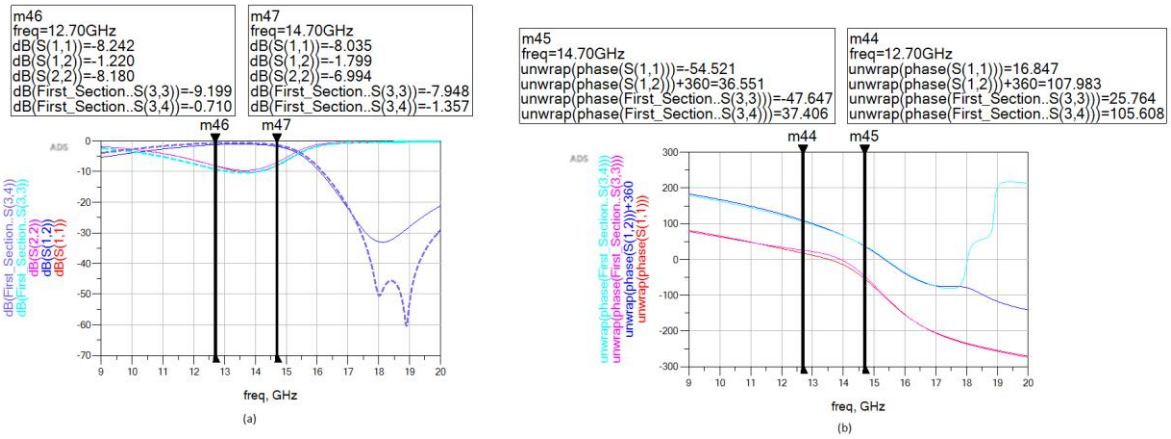

Figure 33. a) Return losses and Transmission losses b) phase for the schematic (dashed lines) and the tuned layout (solid line).

After this, to get an even more accurate result, the resulting layout is parametrized and a component is created (Figure 29(b)). The coupled line section is replaced for this component and a small adjustment is made again (Figure 34).

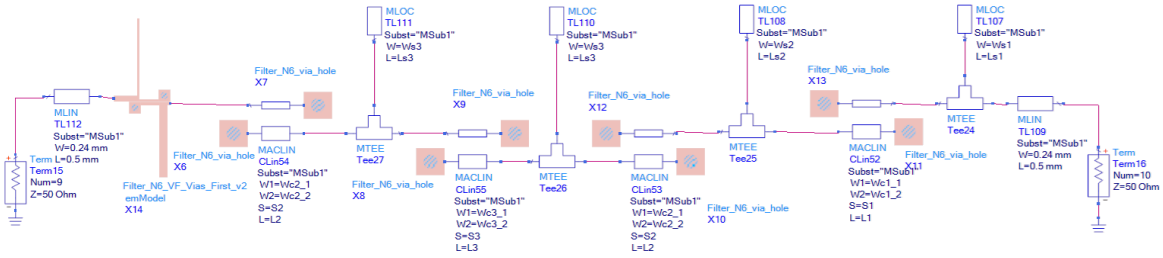

Figure 34. Schematic based on coupled lines with via-hole ground with the first coupled line section and the two open-ended stubs substituted by the layout component

Finally, the final layout for the first coupled section can be found in Figure 29(c) and the final dimensions can be seen in the following tables:

Table 13. Dimensions of the first coupled line section and the two open-ended stubs

Parameters	$MCLIN_1$
W_CL_1 (µm)	50
W_CL_2 (µm)	75
Gap (S) (µm)	12
Length (L) (µm)	440

Parameters	$MLOC_1$	$MLOC_2$
W_s (µm)	50	165
Length stub (L_s) (mm)	1.74	1.55

Now, the second stage corresponds to Figure 35, which is composed by the second coupled line and the third stub; the initial layout can bee seen in Figure 38(a)

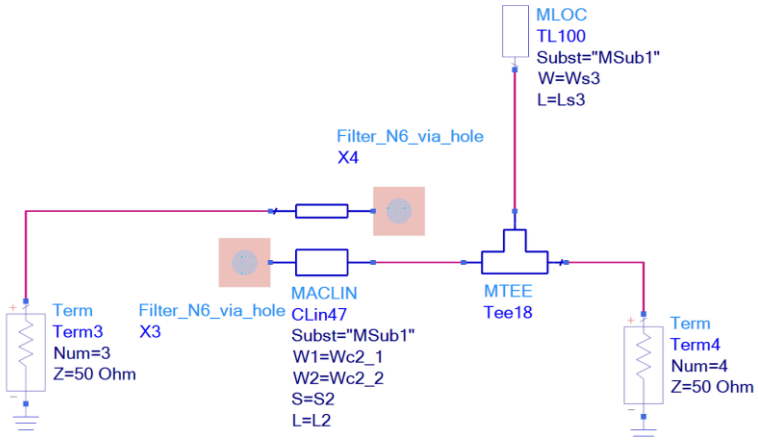

Figure 35. Schematic of the second coupled line section and one open-ended stubs

The way to proceed is the same as the first section, so the results after tuning are the following:

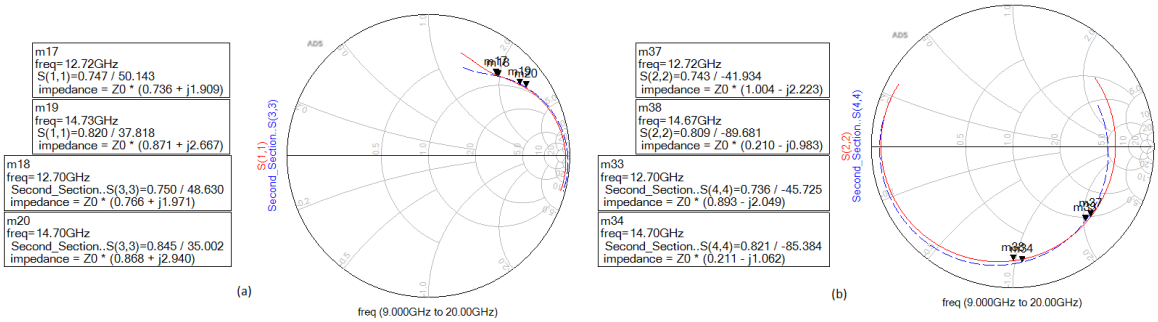

Figure 36. a) S11 b) S22 schematic impedance (blue) and tuned layout impedance (red) on a smith chart.

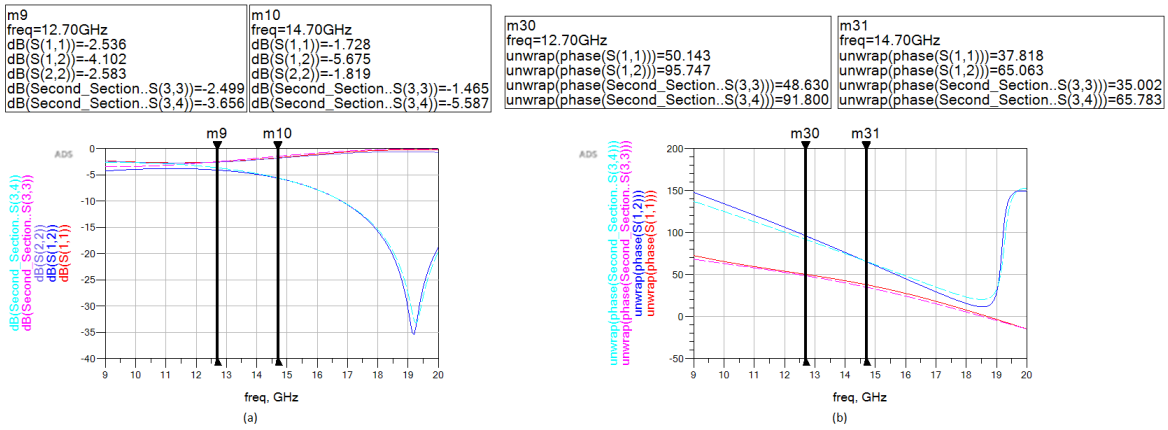

Figure 37. a) Return losses and Transmission losses b) phase for the schematic (dashed lines) and the tuned layout (solid line).

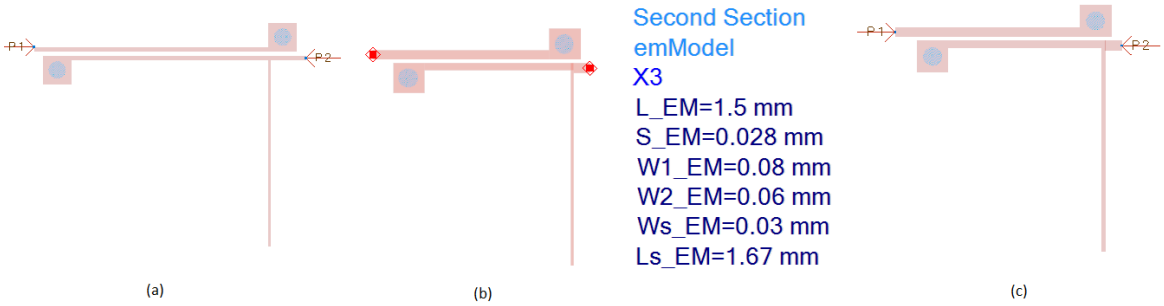

Figure 38 a) Initial layout b) layout component c) final layout of the second coupled line section and one open-ended stub

Then, in Figure 38(b) and Figure 38(c) it can be seen the component model and the final layout. In Table 14 the obtained section dimensions are shown.

Table 14. Dimensions of the second coupled line section and the open-ended stub

Parameters	**MCLIN$_2$**
W_CL$_1$ (µm)	80
W_CL$_2$ (µm)	60
Gap (S) (µm)	28
Length (L) (µm)	1500

Parameters	**MLOC$_3$**
W$_s$ (µm)	30
Length stub (L$_s$) (mm)	1.67

And the third and the last section only is composed by the third coupled line (Figure 39).

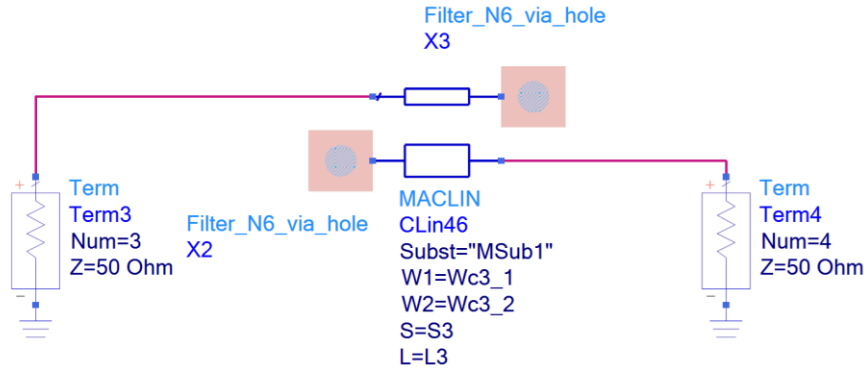

Figure 39. Schematic of the third coupled line section

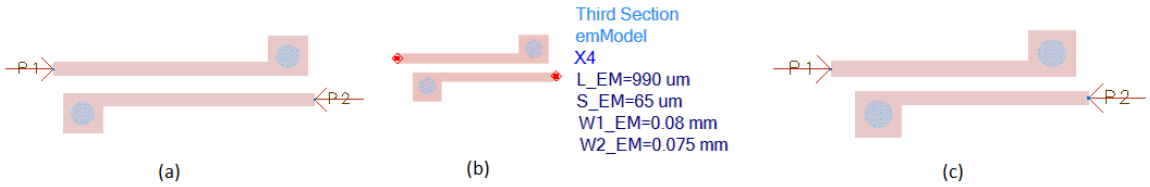

Figure 40 a) Initial layout b) layout component c) final layout of the third coupled line section

Doing the same steps that previously we obtain the initial generated layout, the component model, the final layout (Figure 40) and the table with the final dimensions (Table 15).

Table 15. Dimensions of the third coupled line section.

Parameters	**MCLIN$_3$**
W_CL$_1$ (mm)	80
W_CL$_2$ (mm)	75
Gap (S) (µm)	65
Length (L) (µm)	990

Once we have the three coupled line sections with the three stubs it can be generated the full layout by joining all the sections (Figure 41). Taking into account, that the first section is the same as the fifth and the second is the same as the fourth, we already have all the sections. After joining it together, the layout model will be imported to HFSS. It will be necessary to tune it again because we have extra couplings and impedance changes that we have not taken into account because the coupled lines layouts have been generated separately. Also some differences will appear because ADS momentum is a 2.5D simulator that does not take into account some effects; instead HFSS is a full 3D which it does take into account these effects when calculating the fields.

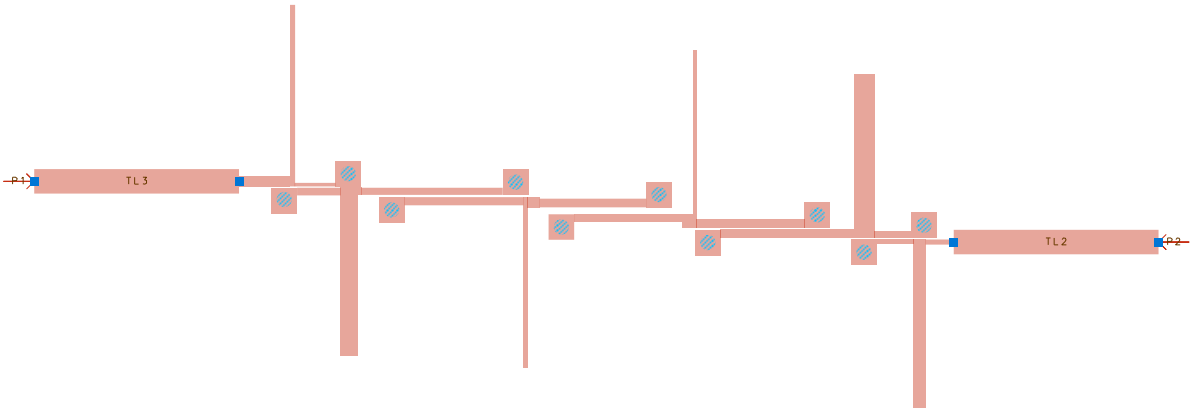

Figure 41. Layout of the filter in Momentum

So after importing the model, which basically is a 2D plane of the layout, several steps must be done to get the 3D model; set the thicknesses needed for each part of the design, create a mechanic or vacuum box, create the wave ports and assign the materials.

After that, the whole model is parametrized to be able to change any dimension quickly. Also, this parametrization will help us to tune the design easily. The tune process can be done changing manually the dimensions until we find the dimensions with which we will obtaining the best response or use the optimetrics option which allows us to make several changes at the same time and try different dimension combinations, basically allow us to do sweeps of several variables at once.

After the tune process, the final layout for the filter can be seen below.

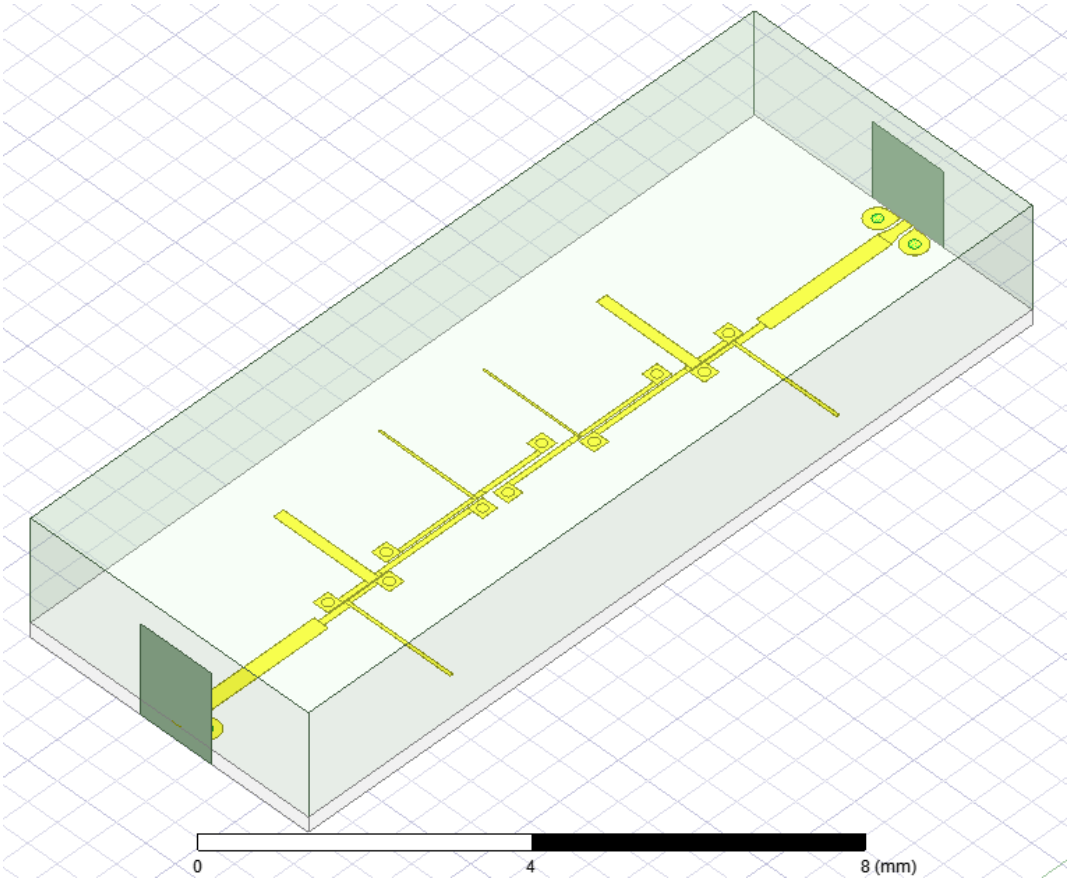

Figure 42. Final Layout in 3D of the filter version A in HFSS

As we can see in Figure 42, the design is very similar to the ADS one but we have add a coplanar pad, the decision to use this is because using this pad the circuit can be measured with a probe station. The reason why it has been discarded to use an SMA connector is because it can add undesired effects such as more insertion losses and changes in the response, having to re-tune the circuit. Apart from this, the manufacturing process also changes since you cannot weld the pin directly on the gold tracks, having to put an extra layer, making the design more expensive and complicated, and also not all manufacturers carry out this type of treatment. In the chapter manufacturing and measurement it will be explained in detail all the information regarded to the measurement system.

Finally, the response of the filter can be plotted after all the steps carried out previously.

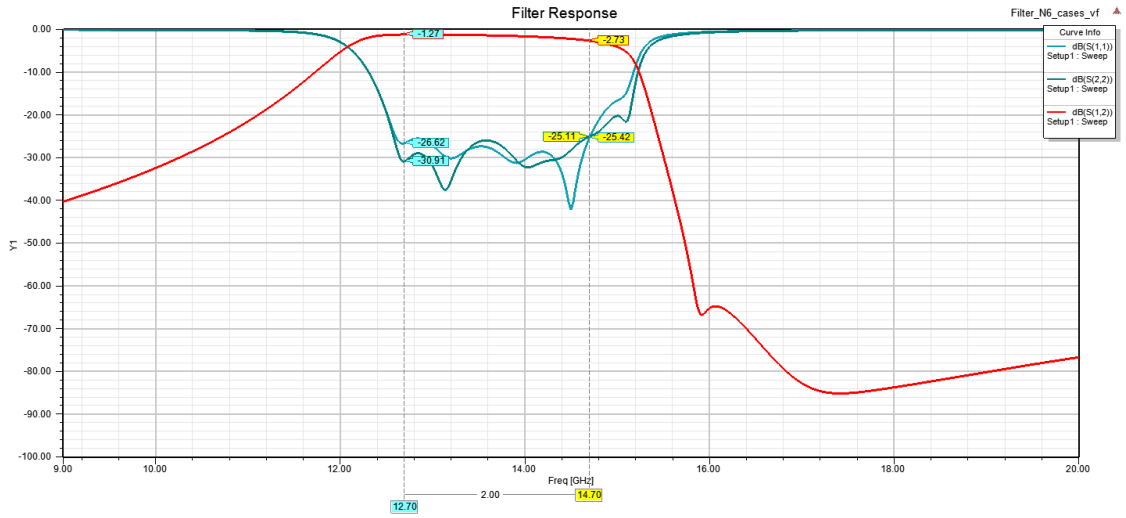

Figure 43. Final Response of the filter A

As can be seen in Figure 43 the filter response accomplishes all the requirements in Table 3. The return losses, $|S_{11}|$ and $|S_{22}|$, are below 25dB and the rejection band levels are also below 40dB. On the one hand, the flatness of the response in the passband is more than 1dB. On the other hand, the transmission zeros do not look as expected, obviously the transmission zeros remains between 18-20 GHz because in this frequency range we have a response below 70dB. This is because there is a feedthrough between the input and the output. This can be understood as that there is an added capacity between input and output causing this degradation in the transmission response. In the following figures we can see what we have stated before.

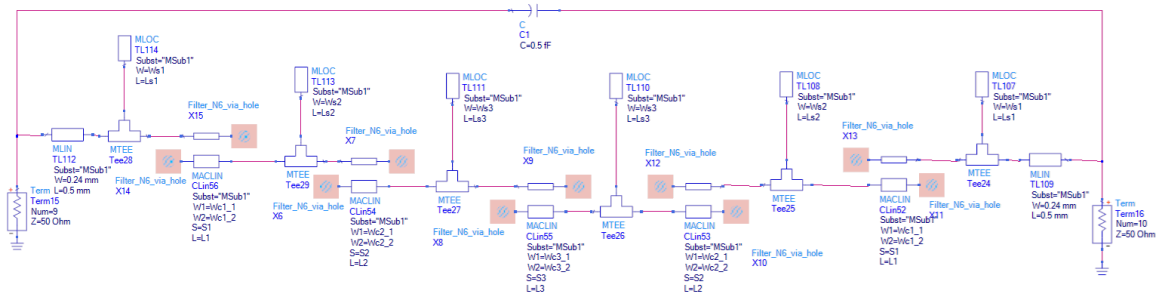

Figure 44. Schematic based on coupled lines with via-hole ground with a capacitance of value 0.5fF between input and output

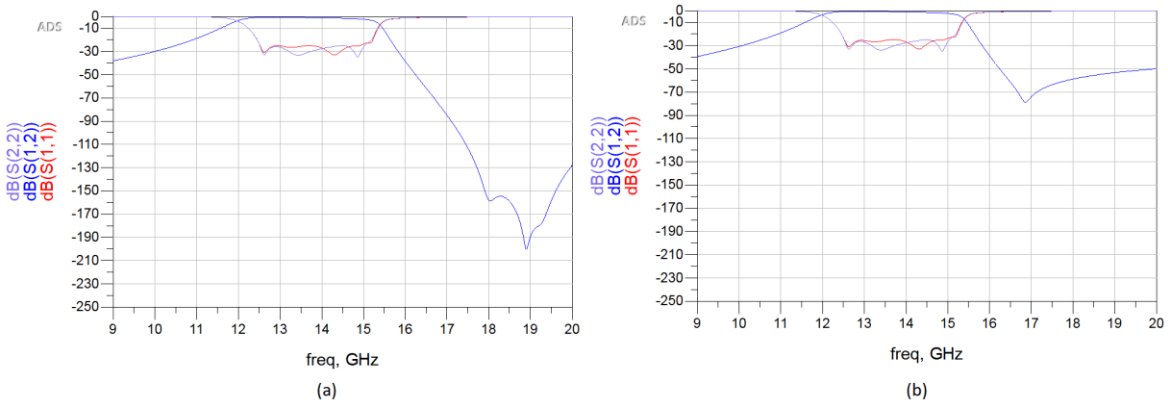

Figure 45. Circuit model S-parameters of filter A (a) Nominal and (b) with an extra capacitance of 0.7fF between the input and the output

So, the way to correct the flatness of the transmission response is by moving the transmission zeros to a higher frequencies, because being the transmission zeros so close we make that there is an abrupt fall that causes this slope, other way to do it is by increasing the bandwidth of the filter, if we do this it is possible to avoid a part of the slope causing us to have less insertion losses. A new model will be designed to try to fix this problem.

Finally, the final dimensions are:

Table 16. Final Dimensions of the filter A

	$MCLIN_1$	**$MCLIN_2$**	**$MCLIN_3$**	**$MCLIN_4$**	**$MCLIN_5$**
W_CL_1 (µm)	80	60	80	60	80
W_CL_2 (µm)	60	80	75	80	60
Gap (S) (µm)	15	32	60	32	15
Length (L) (µm)	525	1580	1060	1580	525

	$MLOC_1$	**$MLOC_2$**	**$MLOC_3$**
W_s (µm)	50	165	30
Length stub (L_s) (mm)	1.72	1.54	1.6

In the following table we have a small comparison of results between the ideal schematic (Figure 15), the real schematic (Figure 25) and the final layout model A (Figure 42):

Table 17. Comparison between ideal schematic, real schematic and final Layout model A.

Parameters	Ideal schematic	Real schematic	Final Layout A
Return losses	>26dB	>25dB	>25dB
Insertion losses	<0.1dB	<1.7dB	<2.8dB
Amplitude balance	<0.05dB	<0.9dB	<1.45dB
Rejection Bands	>50dB at 9 GHz	>40dB at 9 GHz	>40dB at 9 GHz
	>100dB at 17 GHz	>100dB at 17 GHz	>70dB at 17 GHz
Envelope	-	-	7.35mmx3.7mm

3.2 Ku Band Filter Model B

As we stated before, in order to fix the flatness issue it will be increased the bandwidth and the transmission zero will be displaced at higher frequencies. It is important to note that is not enough just short the stubs, because the coupled lines are adjusted for a specific stubs with a given length and width, then if we change the stubs dimensions it is necessary to redo all the design from scratch.

So, applying all the steps in 3.1 but in this case increasing the bandwidth until 15.3GHz (superior band) and positioning for transmission zeros at 19 GHz and two more at 28 GHz, we can obtain the following schematic and his response:

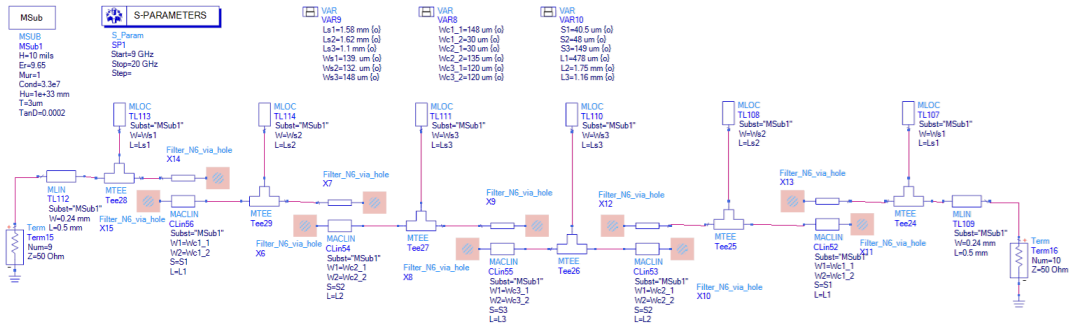

Figure 46 Schematic based on coupled lines with via-hole ground Model B

As we can see in Figure 47, the flatness has been improving having less than 0.5dB. Regarding the return losses and the rejection band levels they meet the proposed specifications, but in this case we have a lower rejection value in the upper band of the filter because we have moved away the transmission zeros.

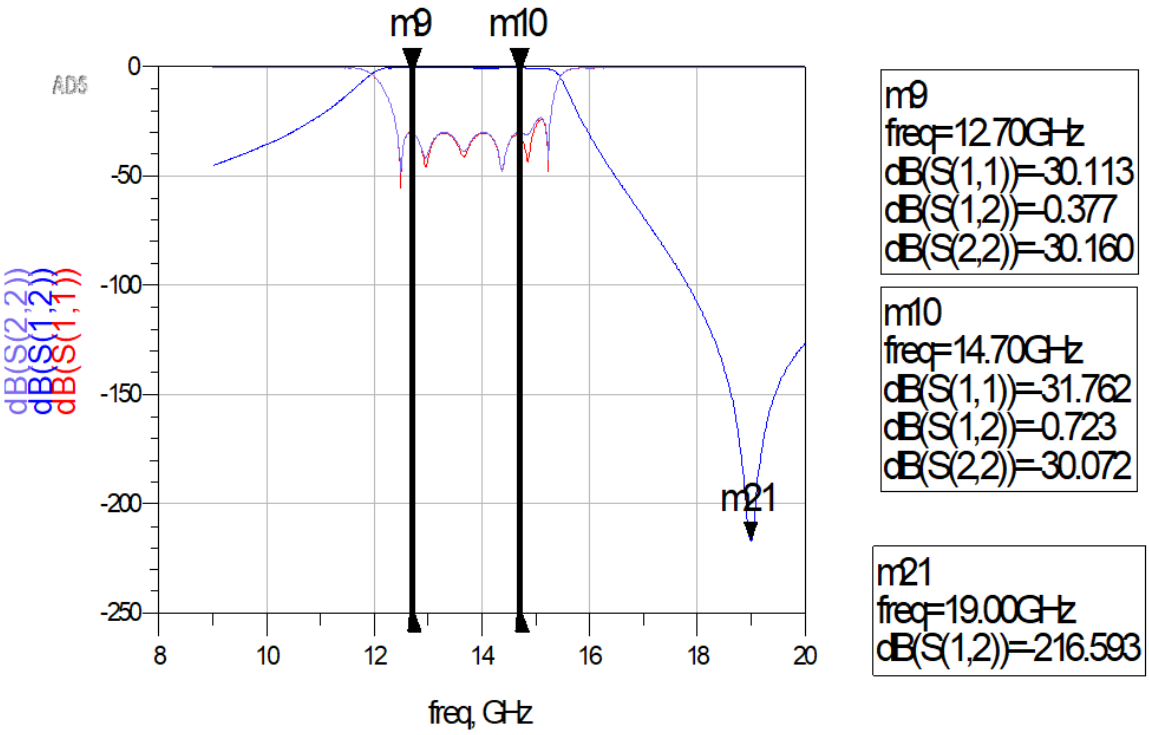

Figure 47. Circuit model S-parameters of the coupled lines with via-hole ground model B solution obtained through optimization

After obtaining the schematic doing the some process to obtain the layout, we obtain the layout in HFSS (Figure 48) and the filter response of the filter (Figure 49).

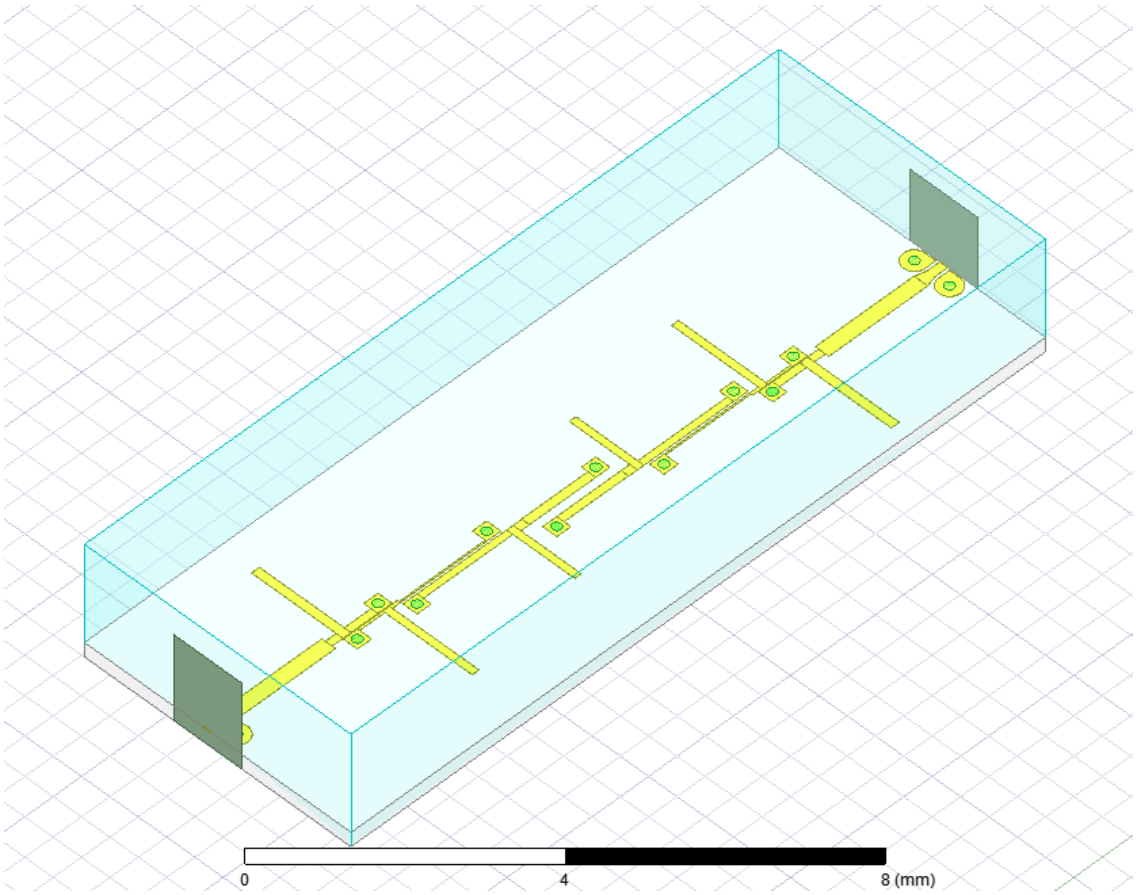

Figure 48. Final Layout in 3D of the filter version B in HFSS

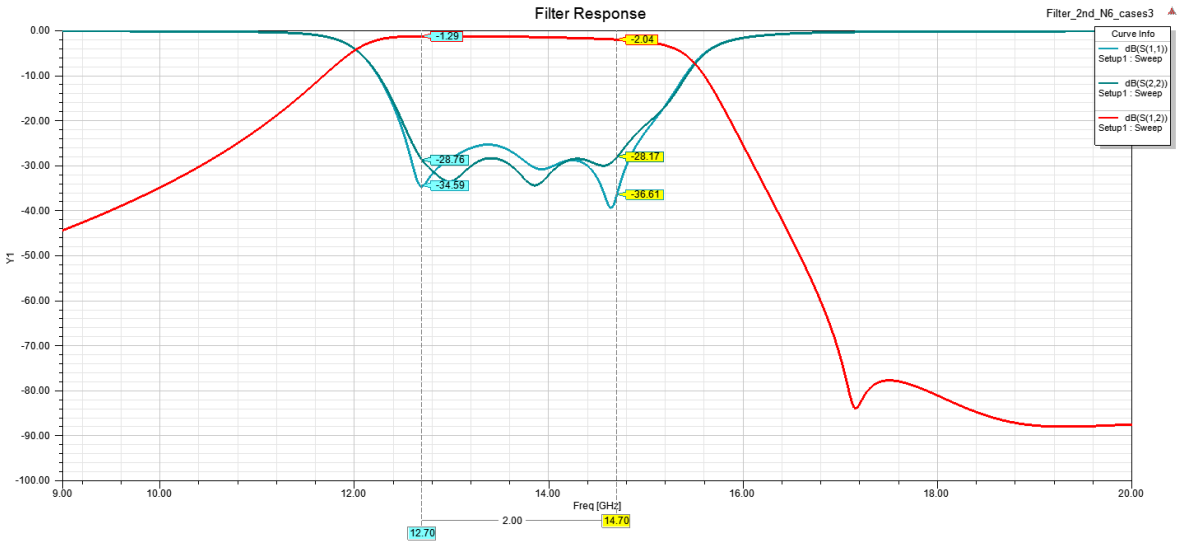

Figure 49 Final Response of the filter B

As we can see, the flatness also has been improved in the layout model, being less than 1dB. The Bandwidth of this model is greater than model A. The requirements continue to be met, where the return losses, $|S_{11}|$ and $|S_{22}|$, are below 25dB and the rejection band levels are also

below 40dB. Regarding to the transmission zeros although we have the same problem the rejection level obtained is enough to accomplish the specifications.

In the following table we have a comparison of results between the ideal schematic the real schematic, the final layout model A and the final layout model B:

Table 18. Parameter comparison between ideal schematic, real schematic, final layout model A and final layout model B.

Parameters	**Ideal schematic**	**Real schematic**	**Final Layout A**	**Final Layout B**
Return losses	>26dB	>25dB	>25dB	>25dB
Insertion losses	<0.1dB	<1.7dB	<2.8dB	<2.1dB
Amplitude balance	<0.05dB	<0.9dB	<1.45dB	<0.75dB
Rejection Bands	>50dB at 9 GHz	>40dB at 9 GHz	>40dB at 9 GHz	>45dB at 9 GHz
	>100dB at 17 GHz	>100dB at 17 GHz	>70dB at 17 GHz	>70dB at 17 GHz
Envelope	-	-	7.35mmx3.7mm	7.9mmx3.9mm

4. Sensitivity

In this section, different worst case analysis (WCA) will be presented. The WCA is used to identify the most critical components or variables which will affect circuit performance. In our case, the variables are basically the fabrication tolerances deviations. Finally, the analysis of the deviation of the via-holes of our design will be compared with those of an interdigital filter to analyze which is more sensitive to the deviation of the via-holes.

4.1 Worst Case Analysis

The first analysis will be focused on the manufacturing tolerances related to the width. Based on the manufacturing tolerances for the Alumina substrates we know that the lines have +/- 3µm of tolerance. This means that in our design, the width, length and separation may have a different value from the one established as nominal. The separation of the lines will be the parameter that will have the most impact of the three variables, because the separation affects to the impedances and the coupling of the coupled line sections. Note that reducing the line 3µm means reducing 1.5 µm on one side and 1.5 µm on the other side and not 3µm on one side.

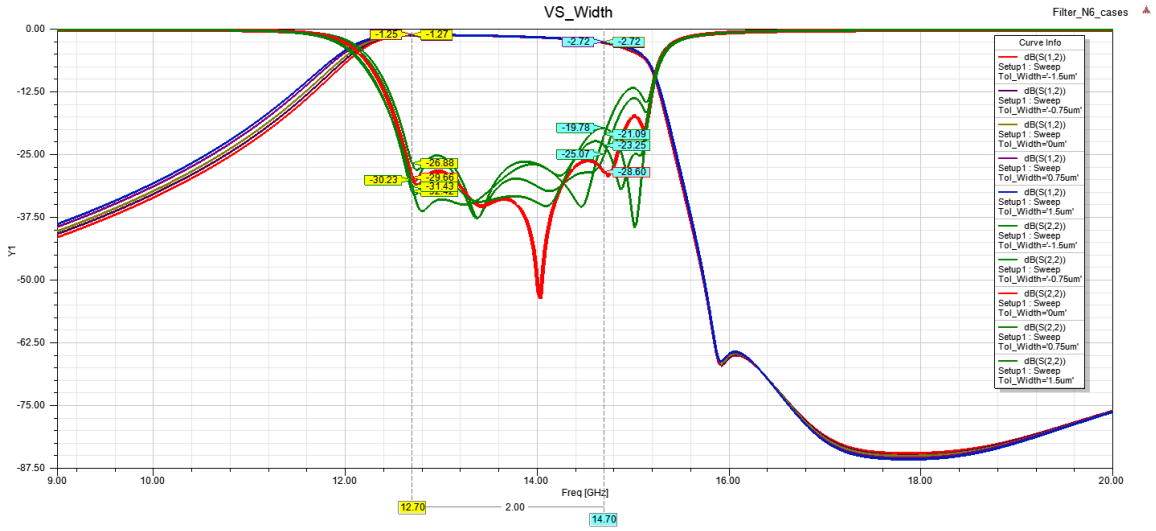

Figure 50. WCA width for the filter A

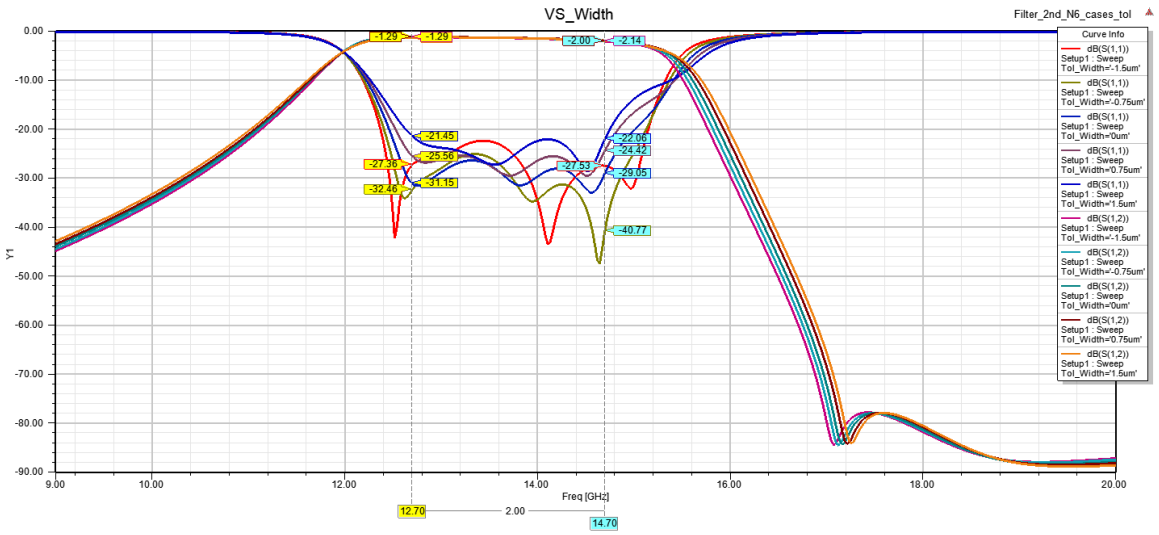

Figure 51. WCA width for the filter B

In Figure 50 and Figure 51, it can be seen the different responses of the filter doing a sweep from -1.5µm to 1.5µm. In both figures the return losses decreases 10dB when we are in extreme cases. Even though we still accomplish the requirements because we have let a big margin.

The second WC analysis will be focused in the via-hole position deviation. This is the most important analysis to take into account because the via-hole is the "structure" that causes the most change to the design. In this case, the tolerances on the via-hole position are +/- 50µm, 17 times higher than the width tolerances. So we can assume that the coupled lines can be lengthened or shortened by +/- 50µm. Keep in mind that this deviation can be both the Y axis and the X axis (Figure 52). This deviation causes that the coupling of all resonators change, doing that the reflection zeros move in frequency causing a degradation of the return loss. In the following figures it can be seen the results of the WC analysis.

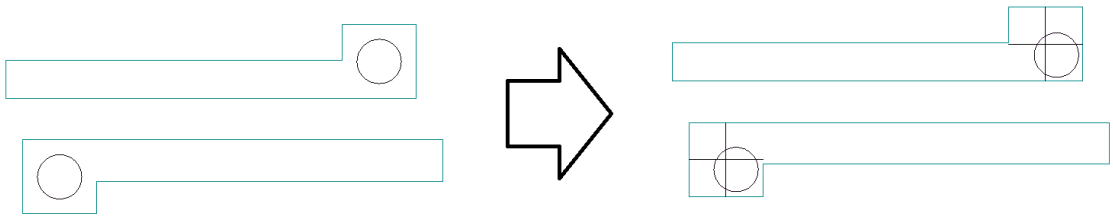

Figure 52. Via- hole position deviation on the X and Y axes

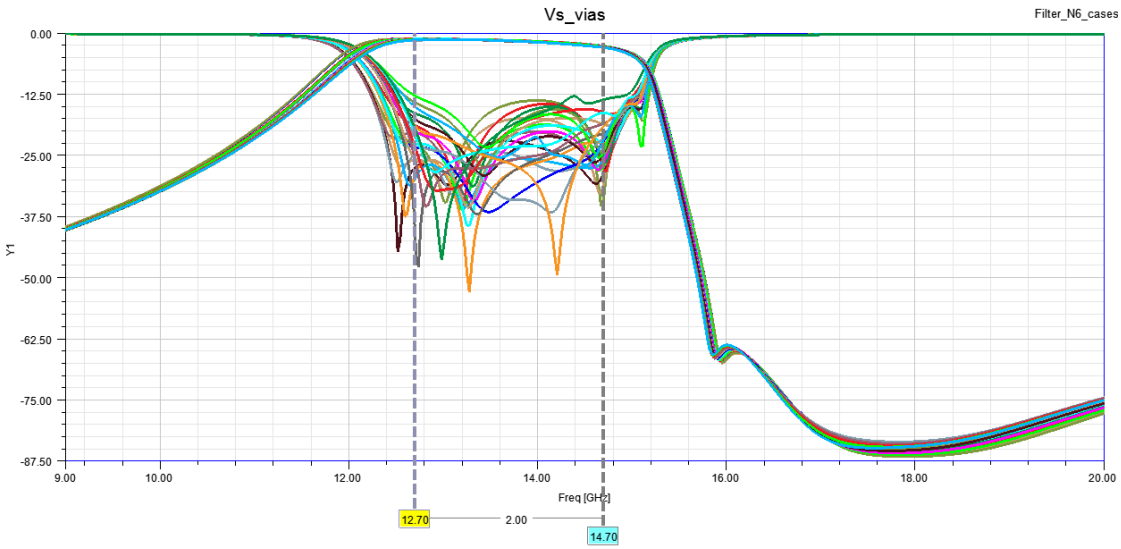

Figure 53. WCA via-hole position for the filter A

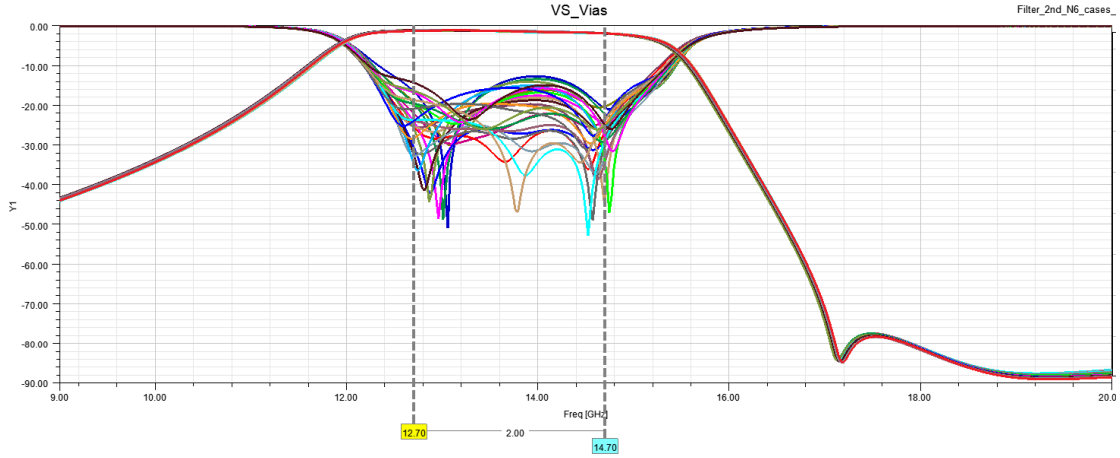

Figure 54. WCA via-hole position for the filter B

What can be seen in both figures is that this deviation tolerances causes a mismatch in the response causing the degradation of the response and the overlapping of the reflection zeros. The worst matching obtained appears when we have a deviation of +50 µm or -50 µm, having -13dB in both cases. As we already knew this from the beginning we choose to have an adaptation of 25dB in order to comply the specifications. Normally, you never expect to get the extreme case of deviation then if we assume 25 µm of deviation we still will accomplish the specifications.

There are several ways to reduce the impact of the manufacturing tolerances but as it is obvious there is always a trade-off. For example if we increase the thickness substrate or we select another type of substrate with a lower permittivity the size of the filter will increase

but the affectation of the manufacturing tolerances will decrease because regarding the same frequency the change of 50 µm or 3 µm is less. In our case, if we make this type of change, we will stop meeting the defined limit dimensions.

The third WC analysis will combine the two previous analysis considering the extreme cases to know what could be the worst adaptation value obtained.

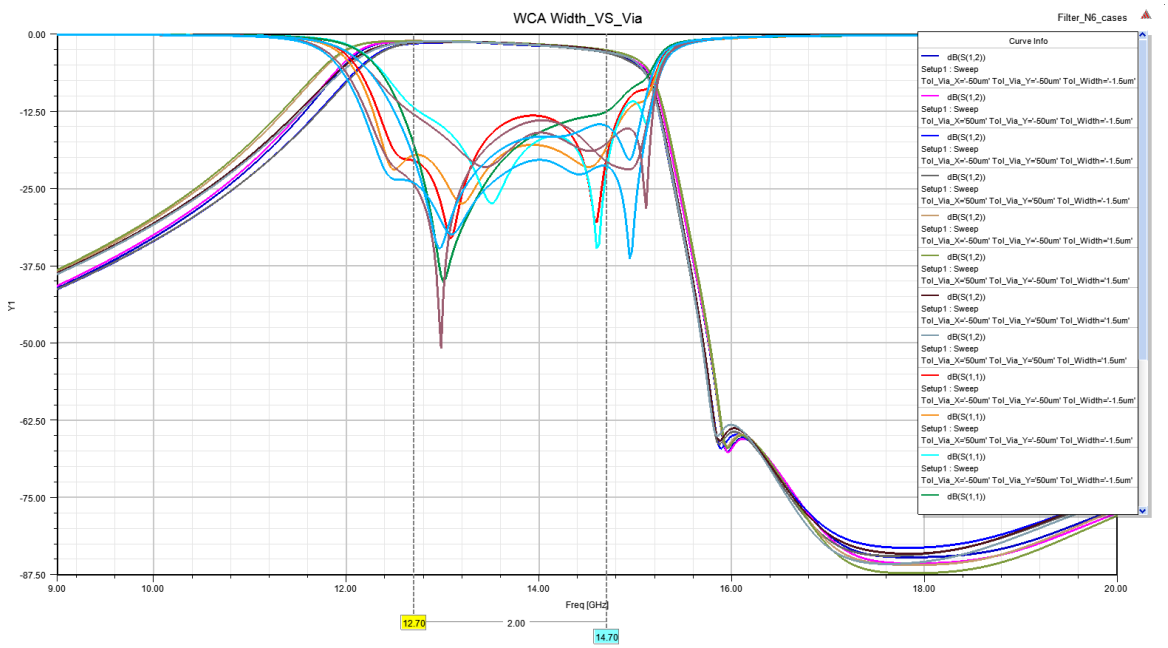

Figure 55. WCA extreme case of width and via-hole position for the filter A

In this extreme case we would not meet the proposed specifications. As we can see Figure 55 is similar to the one with the via-hole deviation analysis (Figure 53), so we can conclude that the via-hole deviation will be the dominant effect on manufacturing tolerances.

4.2 Sensitivity comparison between our filter vs Interdigital filter

After carrying out all the WCAs, in order to know if our filter is less sensitive depending on the positioning of the via-holes, we have chosen to compare the different results of the positioning analysis between our filter and an interdigital filter like the one in Figure 56.

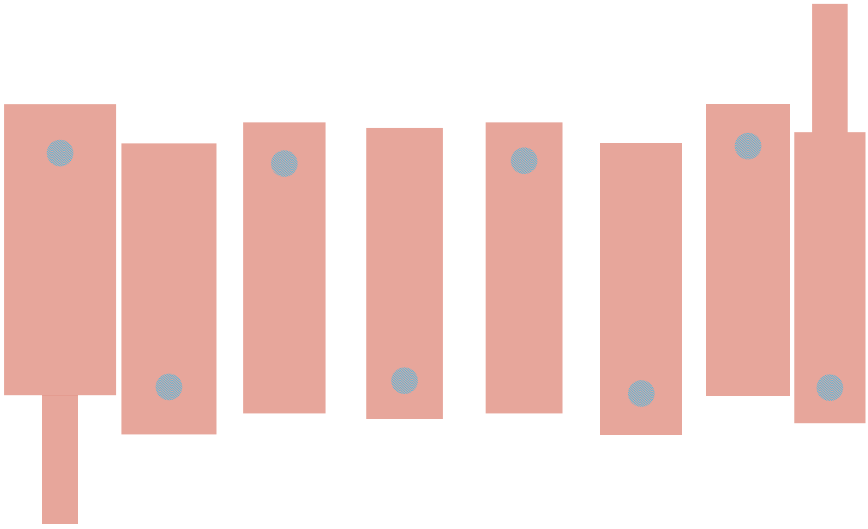

Figure 56. Interdigital filter of order 6

The worst case analysis for the via-hole position deviation can be seen in the next figure:

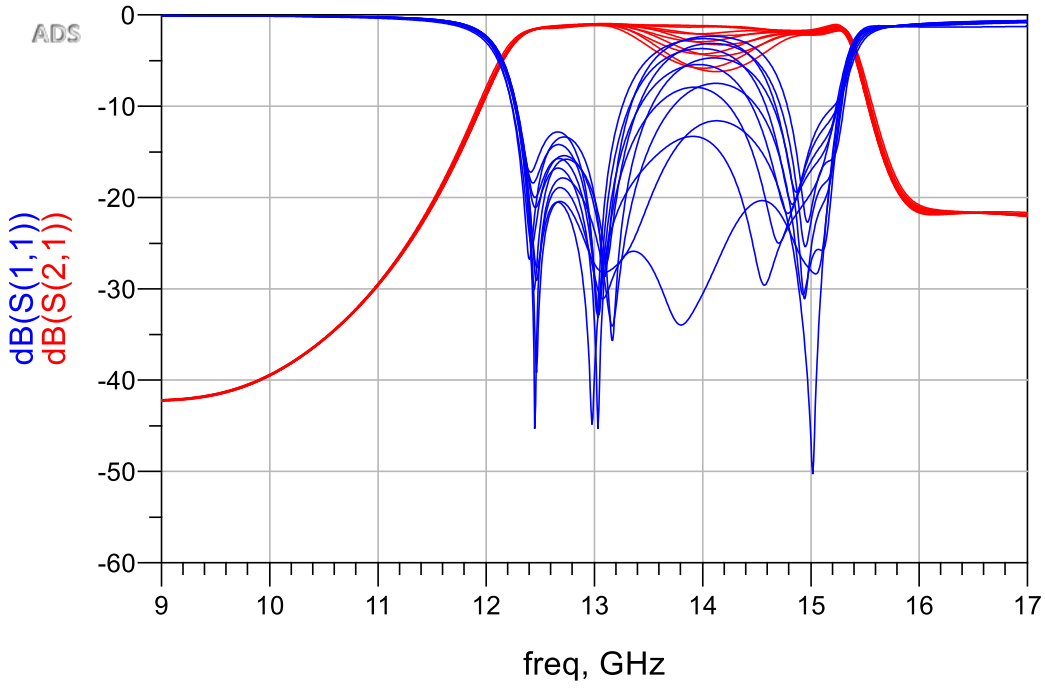

Figure 57. WCA via-hole position for Interdigital filter of order 6

To make this comparison, we have use the MSE estimator for each position of the via-holes. So, we have been able to extract the following graph:

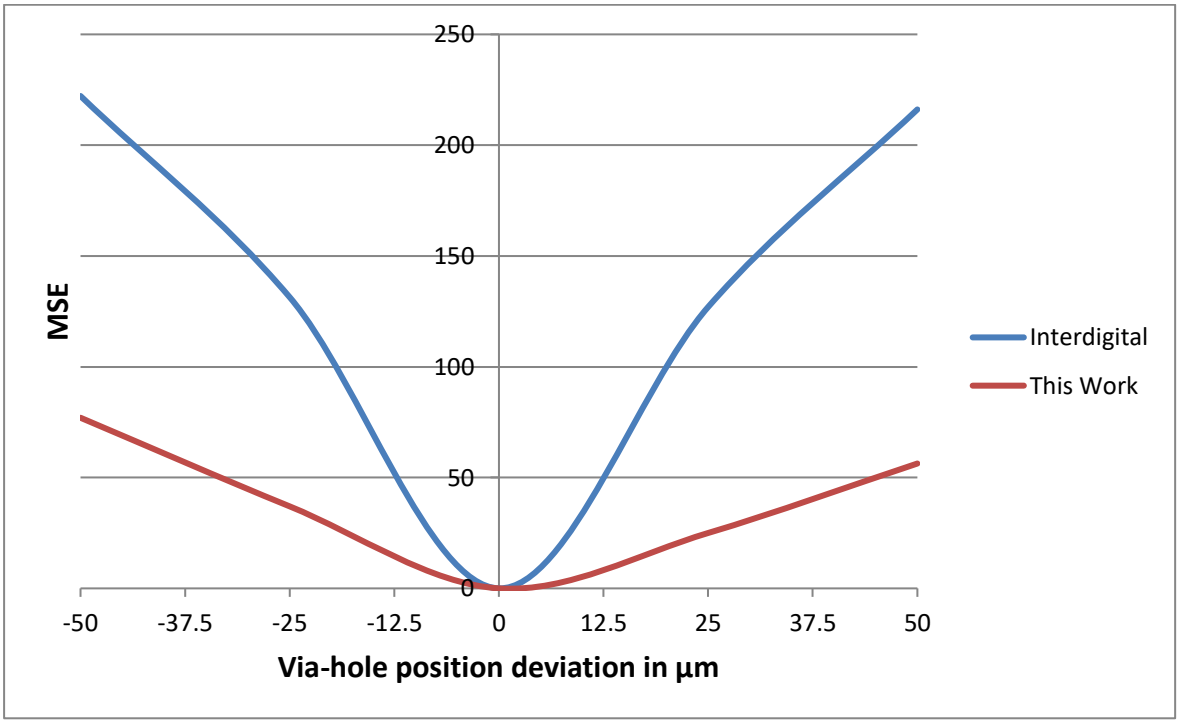

Figure 58. Comparative graph between the deviation of the via-holes in our filter and an interdigital filter

As we can clearly see in Figure 58, our filter is less sensible to the deviation of the via-holes. This is mainly due to the fact that 4 of the 6 resonators used in this topology are lambda / 2, so the variation that causes the via-hole is lower than that of the interdigital filter whose resonators are lambda/4. Another reason is, as we stated at the beginning of the work, that each coupled section is independent of the others and therefore, the response should be less affected by the displacement of the via-holes.

5. Manufacturing and measurement

In this last chapter, the last two models designed in the previous section will be implemented, the model A and the model B. Once the layout in HFSS is finished, the edge layer that will determine the cutting lines of the substrate is added and finally it is exported into .DXF to be sent to manufacture to Thin Film Products, TFP.

Once manufactured, through the coplanar pad we can measure our equipment with probes with the following machine:

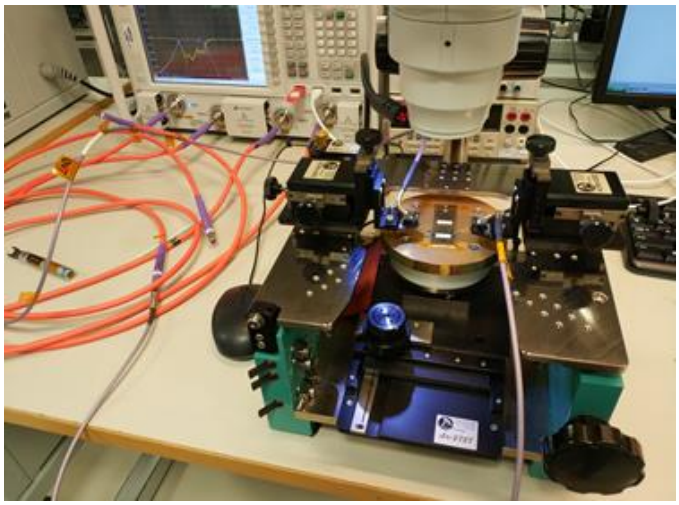

Figure 59. Probe station to measure the substrates with pico probes

To measure the S parameters of the network, the Agilent PNA-X N5242A Vector Network Analyzer (VNA) in conjunction with the tip machine will be used.

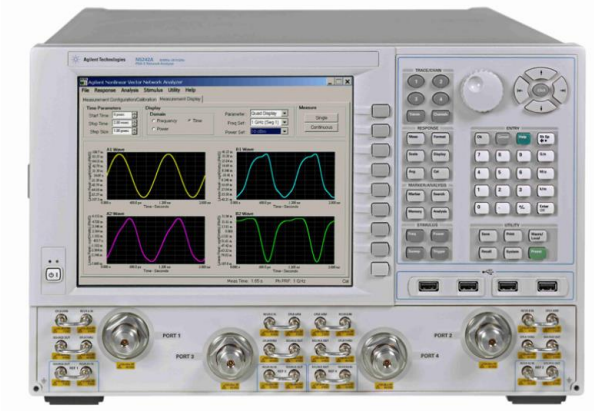

Figure 60. Agilent PNA-X N5242A

Before carrying out any measurement, we will have to configure the frequency range to simulate; in this case it will go from 9GHz to 20GHz with a resolution of 1MHz. After this it is necessary to calibrate the equipment with the calibration substrate for the probes CS 2-150 GSG.

(a) (b)

Figure 61. a) CS-2-150 pico probes b) Calibration substrate for CS-2-150

Once the measurement has been made, the data will be exported in touchstone format (.S4P) and added to ADS or Matlab to visualize the results and compare them with the simulations.

5.1 Model A

The first manufacture model of the filter can be seen in the next figure:

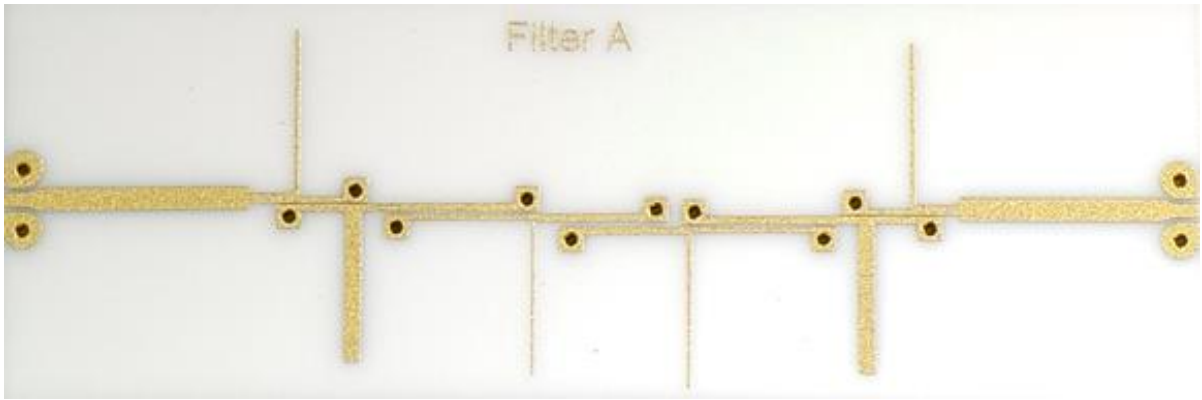

Figure 62. Filter model A

In Figure 63 the response of this filter is shown:

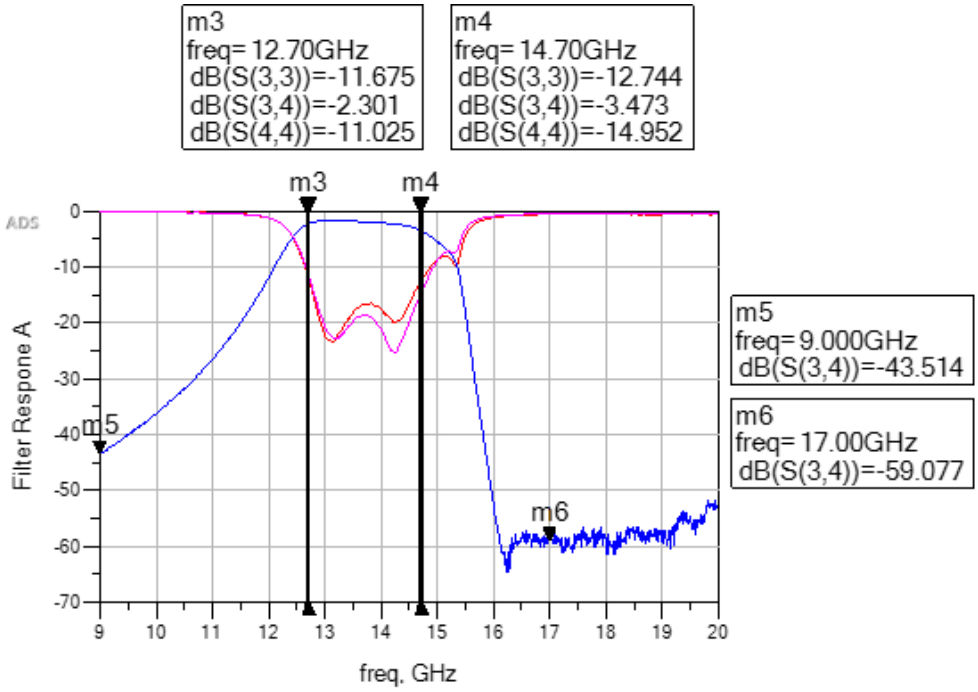

Figure 63. Measured response of the filter A

As we can see in the response the returns losses of the filter are worse than the nominal case of this filter, being ≥ 11dB in the whole Band. Also, we can see that the response of the filter seems to be syntonised and the transmission zeros have been overlapped and moved in frequency, causing a reduction in the bandwidth of the filter. Regarding to the insertion losses, apart from being ≥ 3dB in the upper band, the flatness is also greater than 1 dB, which is what we check by simulation.

This degradation in the response will be mainly caused by the tolerances of the position via-holes and by the tolerances in the separation between the lines. As we said before we are working in the limits of the design rules so the tolerances can affect a lot due to the manufacture processes. Also, if the design is observed with a microscope of a higher pressure we can see other curiosities of this manufacture as the lines are not completely straight but are corrugated, it can affect the separation of the lines, and another example is that the ways are not all totally round or of the same diameter.

It will be studied in detail the possible manufacturing tolerances in order to correlate the measure with the simulation results as future work.

5.2 Model B

The second model has the following manufacture figure:

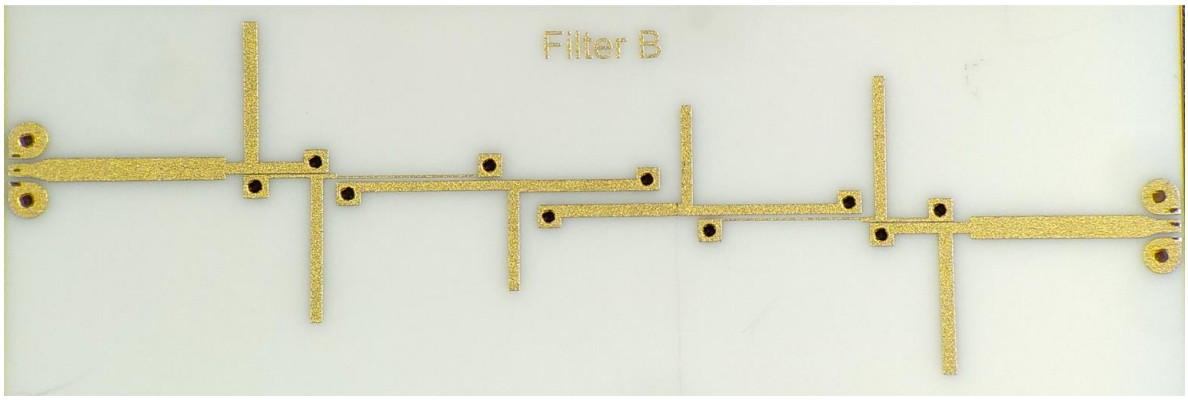

Figure 64. Filter model B

The response of this second model is the following:

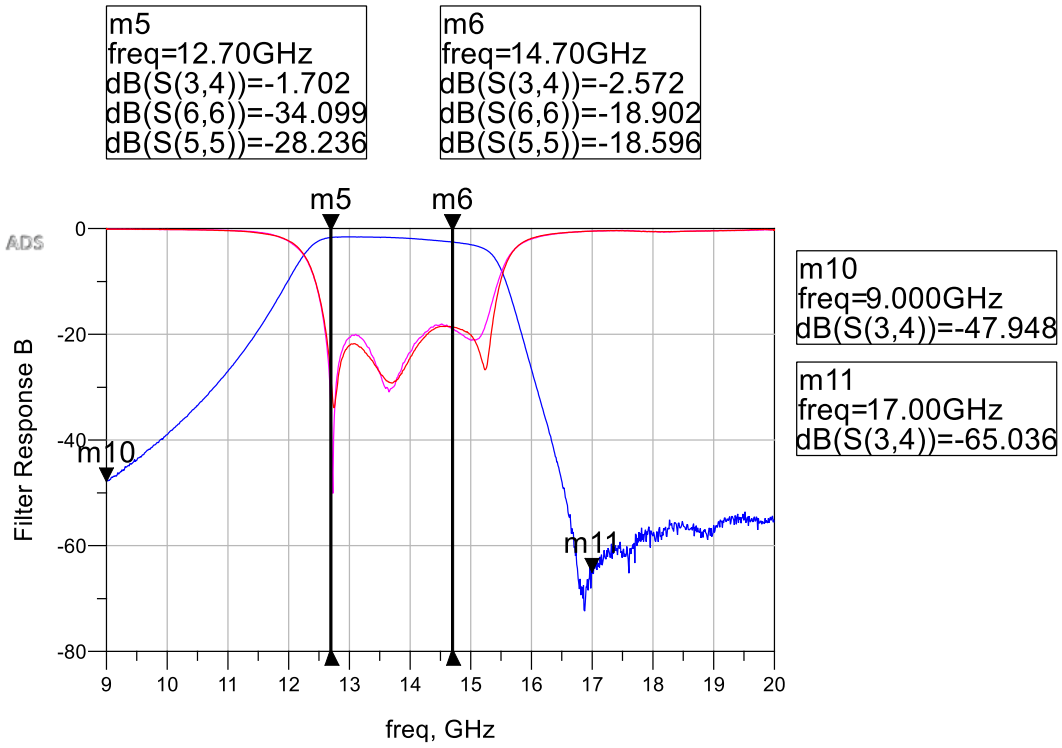

Figure 65. Measured response of the filter B

In Figure 65 can be seen that in this case we have a response with return losses greater than 18dB and flatness less than 1dB. So, we fulfil the condition of flatness that we set out to achieve with this second design by moving the transmission zeros away and we comply with all the electrical specifications of Table 2. Anyway, this model B will be analyzed in order to correlate the simulation results and the measures.

Table 19. Nominal values vs manufactured values

Parameter	Nominal Value	Manufactured Value	Tolerance Value
Separation between line	10 µm for Section 1 38 µm for Section 2 140 µm for Section 3	14 µm for Section 1 43 µm for Section 2 145 µm for Section 3	+/- 3µm
Width	-	+2 µm	+/- 3µm
Via-hole diameter	150 µm	165 µm	+/- 25µm
Position of via hole	0 x axis 0 y axis	-8 µm x axis -8 µm y axis	+/- 50µm

If we do the simulation changing the values that we can see in Table 19 will get a response that closely resembles the measure.

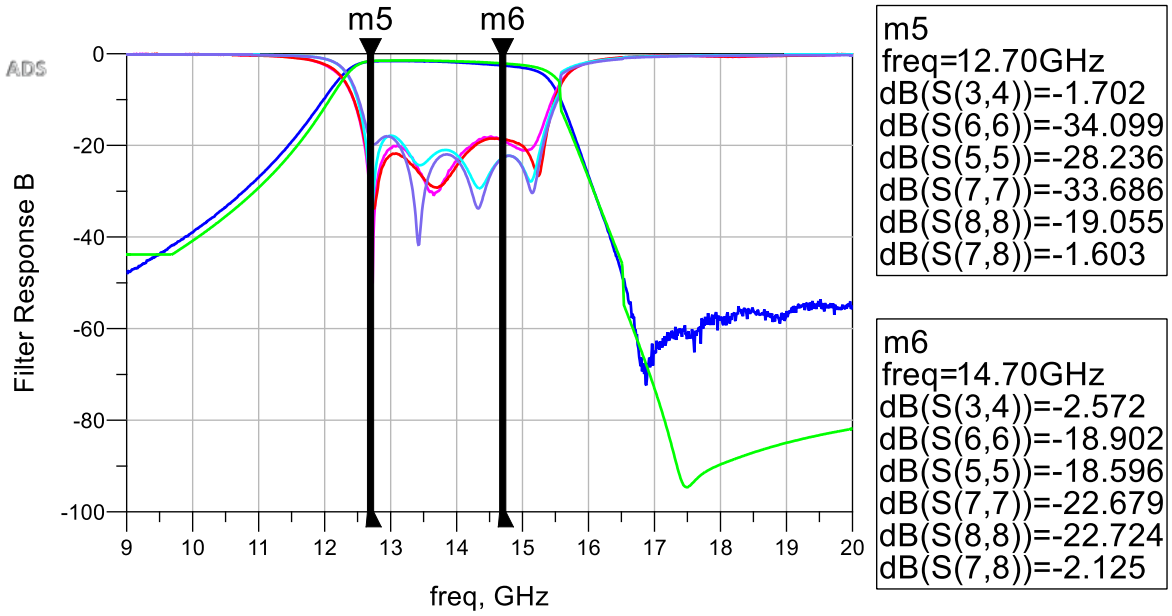

Figure 66. Measured response of the filter B (solid lines) vs simulated response with the corrections in table 19 (dashed lines).

So as we can see in Figure 66, the differences that still remains between the simulated response and the measured response can be caused by other factors as the via holes not are perfectly round, the calibration, the lines are not completely straight or other effects

produced by designing in the limit of the design rules. Also, as we mentioned for the model A and we have been able to check the tolerances in the via-holes and the separation between the lines have been those that have caused the degradation of the response.

5.3 Comparison of Various Coupled Line Tx-Filters

Taking as reference the results of the filter B, we can compare the performance of the filter with other filters that works in the same frequency. In Table 20, we have another TX-Filters extracted from the source [2]

Table 20. Comparison of Ku Band filters realized on Alumina substrate

	f_L (3 dB) GHZ	**f_U (3 dB) GHZ**	**FBW (3 dB) %**	**IL dB**	**RL dB**	**Group delay ns**	**Size mm**
CLF	12.5	16.16	28.6	1.5	13	0.2±0.03	9x2
Hairpin	13.1	15.2	14.8	1.5	20	0.38±0.04	10x6
ringresonator	13.7	15.1	9.7	2.2	17	0.64±0.06	7x2.5
Interdigital	13.2	14.78	11.2	2.2	10	0.48±0.03	3x3
This work	12.4	15	17.3	2.5	18	0.4±0.05	8x4

As we can see in general terms the performance of our filter is better than the other ones. Regarding to the size is true that our filter is large compared to the other ones, but is because we have used stubs in order to generate transmission zeros in the upper band and also the order of the other filters are 3 and 4. However, the Y size, 4 mm, can be reduced up to 2.5mm by folding the stubs.

6. Conclusions and further work

In this final master thesis a Ku Band filter based on NRN topology has been studied, designed, manufactured and measured. The specifications for the model B have been achieved both in band rejection levels and in return losses along a bandwidth of 17.5%, the results being slightly higher than the existing proposals. Table 21 resumes the statement of compliance for the filter B. In addition, the sensitivity of the filter obtained has also been studied, checking that the topology selected is less sensitive to the positioning of the via-holes than another topology such as the interdigital one, which also uses the via-holes.

Table 21. Statement of compliance for filter model B

Parameters	Specified	Measured	Remarks
Frequency	12.7-14.7 GHz	12.4-15 GHz	Increase of 5%
Return losses	>15dB	>19dB	At ambient temperature 25ºC
Insertion losses	<3dB	<2.6dB	Condition proposed later
Amplitude balance	<1dB	<0.9dB	Condition proposed later
Rejection Bands	>40dB at 9 GHz	>47dB at 9 GHz	
	>40dB at 17 GHz	>55dB at 17 GHz	
Envelope	8mmx4mm	7.9mmx3.9mm	The size can be reduced by folding the stubs

Due to the limited time to deliver the work, it has not been possible to bring the real measure closer to the obtained simulation, this means, to eliminate the small displacement in frequency or the appearance of other reflection zeros, or to find out the reason for the difference in transmission in the upper band observed in the measurement with respect to the simulated.

On the one hand, it would be possible to complete a more exhaustive analysis trying to find the why of the issues stated before and do the correlation between the measure and the simulation for the model A. Also it could be reduced the size of the two models by folding the stubs and see the changes that this causes, which should be minimal, since the only thing that should change are the stubs themselves but they keep maintaining the same impedance and electrical length.

On the other hand, we have also fulfilled the objectives of familiarizing ourselves with the process of designing this type of microwave devices, starting from the initial idea to checking the manufactured result, going through all the phases of analysis and simulation.

7. Bibliography

[1] M.F. Islam, M.A. Mohd Ali and B. Yeop Majlis, “Miniaturized Bandpass Filter for Ku-band Applications”, *5th Student Conference on Research and Development*, SCOReD 2007 Proc. ELE-19, 11-12 December 2007, Bangi (PERMATA), Malaysia

[2] Daniel Maassen, “Design and Comparison of Various Coupled Line Tx-Filters for a Ku-Band Block Upconverter”, GeMiC 2016, March 14–16, 2016, Bochum, Germany

[3] Y. Li, L. Hu, J. Chen, Y. Fei, ”A Ku-Band Hairpin Filter Based on LTCC Technology,” in Microwave Conference, pp. 478-480, Sept. 2008.

[4] C. Y. Chang and D. C. Niu, “A novel CPW interdigital filter,” in Asia–Pacific Microw. Conf. Dig., Dec. 2001, pp. 621–624

[5] David M. Pozar, Microwave Engineering, John Wiley & Sons, Inc., 2005.

[6] G.C. Temes and S. Mitra, Modern Filter Theory and Design, John Wiley & Sons, Inc., 1973.

[7] C. Kudsia R. Cameron and R. Mansour, Microwave filters for communications systems: fundamentals, design, and applications, Wiley, 2007.

[8] S. Amari and G. Macchiarella, “Synthesis of inline filters with arbitrarily placed attenuation poles by using no resonating nodes,” IEEE Transactions on Microwave Theory and Techniques, vol. 53, no. 10, pp. 3075-3081, Oct 2005.

[9] Yuxing He, “A Coupling Matrix and Admittance Function Synthesis for Mixed Topology Filters,” IEEE Transactions on Microwave Theory and Techniques, vol. 64, no. 12, Dec 2016.

[10] J.-H. Park, S. Lee, and Y. Lee, “Extremely miniaturized bandpass filters based on asymmetric coupled lines with equal reactance,” IEEE Transactions on Microwave Theory and Techniques, vol. 60, no. 2, pp. 261–269, Feb. 2012.

[11] [G. L. Matthaei, L. Young, and E. M. Jones, Microwave Filters,Impedance-Matching Network, and Coupling Structures. Dedham, MA: Artech House, 1980.

[12] S.-S. Myoung and J.-G. Yook, “A miniaturized method of parallel coupled- line filters using lumped capacitors and grounding,” in *35th Eur. Microw. Conf. Dig.*, Oct. 2005, p. 4.

[13] V. K. Tripathi and C. L. Chang, “Quasi-TEM parameters of non-symmetrical coupled microstrip lines,” *Int. J. Electron.*, vol. 45, no. 2, pp. 215–223, Aug. 1978.

[14] S. Amari, “Capacitance and inductance matrices of coupled lines from modal powers,” *IEEE Trans. Microw. Theory Tech.*, vol. 41, no. 1, pp. 146–150, Jan. 1993.

[15] F.-L. Lin, C.-W. Chiu, and R.-B. Wu, “Coplanar waveguide bandpass filter—A ribbon-of-brick-wall design,” *IEEE Trans. Microw. Theory Tech.*, vol. 43, no. 7, pp. 1589–1596, Jul. 1995.

[16] P. K. Ikalainen and G. L. Matthaei, “Wide-band, forward-coupling microstrip hybrids with high directivity,” *IEEE Trans. Microw. Theory Tech.*, vol. MTT-35, no. 8, pp. 719–725, Aug. 1987.

[17] D. G. Swanson, “Grounding microstrip lines with via holes,” IEEE Trans., MTT-40, August 1992, 1719–1721.

[18] Dr. Greiner “Design rules for thin-film substrates”, 21 September 2007

[19] Microwaves & RF. 2016. What’s the Difference Between Microstrip and Stripline?. [ONLINE] Available at: https://www.mwrf.com/active-components/what-s-difference-between-microstrip-and-stripline. [Accessed 1 February 2019].

[20] GOLDFARB M. E. AND PUCEL R. A., “Modeling via hole grounds in microstrip,” IEEE Microwave and Guided-Wave Lett., vol. 1, no. 6, pp. 135-137, June 1991.

[21] HE X., LEI Z., WANG Q., “Transmission characteristics of via holes in high-speed PCB”, International Synonym on Antennas and Propagation (ISAP), 2013.

[22] Ghulam Mustafa Khan Junejo, “Experimental Analysis of Via-hole-ground Effects in Microwave Integrated Circuits at X-band”, POSTER 2015, PRAGUE MAY 14